Journal Name

ARTICLE TYPE

Cite this: DOI: 10.1039/xxxxxxxxxx

Modeling Excitation Energy Transfer in Covalently Linked Molecular Dyads Containing a BODIPY Unit and a Macrocycle: Electronic Supplementary Information (ESI)

Cloé Azarias,[a] Lorenzo Cupellini,[b] Anouar Belhboub,[a,c] Benedetta Mennucci,*[b] and Denis Jacquemin*[a,d]

[a] *Chimie Et Interdisciplinarité, Synthèse, Analyse, Modélisation (CEISAM), UMR CNRS no. 6230, BP 92208, Université de Nantes, 2, Rue de la Houssinière, 44322 Nantes, France. E-mail: Denis.Jacquemin@univ-nantes.fr*

[b] *Dipartimento di Chimica e Chimica Industriale, University of Pisa, Via Moruzzi 3, 56124 Pisa, Italy. E-mail: Benedetta.Mennucci@unipi.it*

[c] *Centre Inter-universitaire de Recherche et d'Ingénierie des Matériaux (CIRIMAT), UMR CNRS no. 5085, Université Paul Sabatier, 118, route de Narbonne, 31062 Toulouse, France.*

[d] *Institut Universitaire de France, 1 rue Descartes, F-75231 Paris Cedex 05, France.*

S1 Definition of the fragments in 1

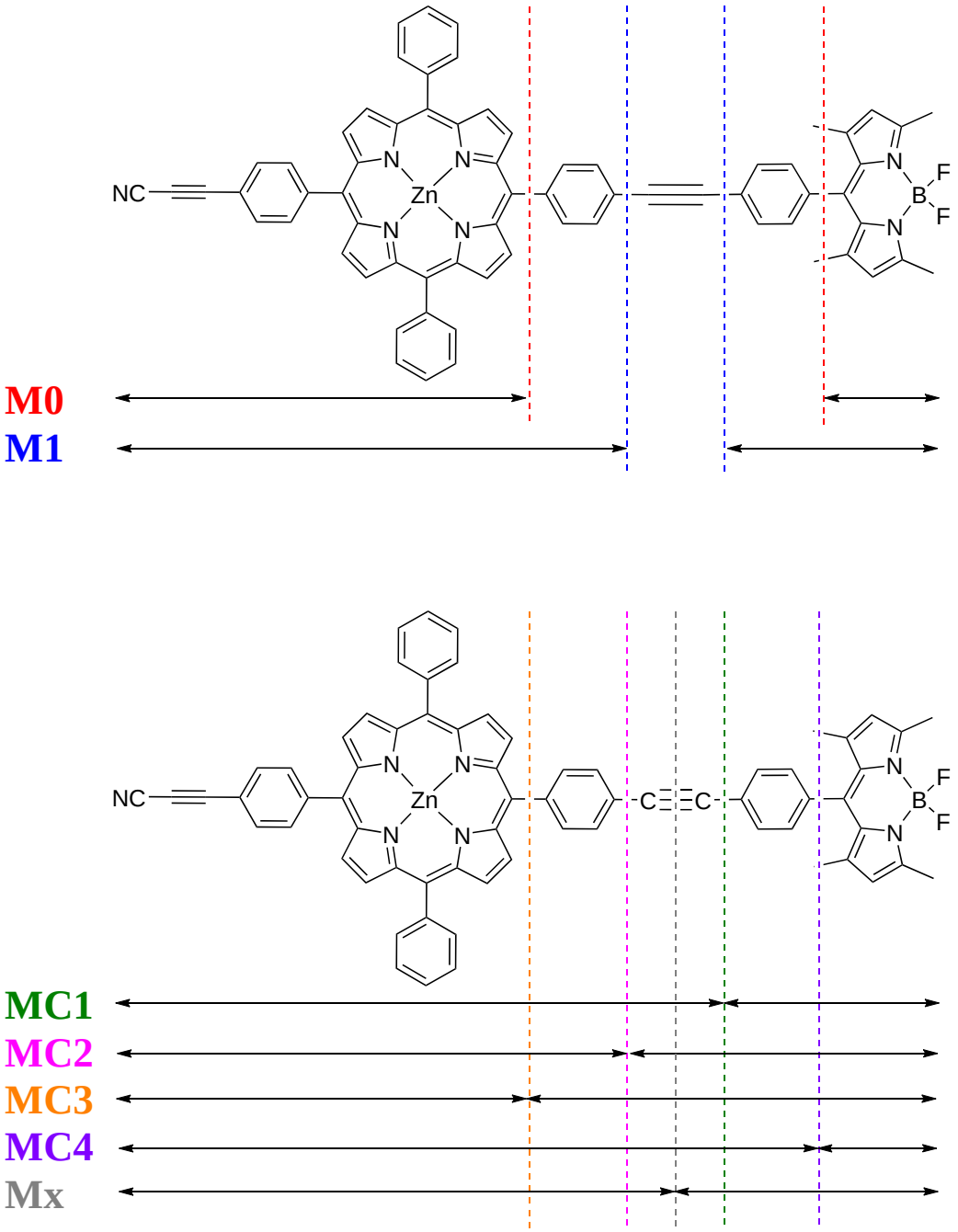

Fig. S1 Representation of the different fragmentation schemes considered in dyad **1**.

Table S1 Theoretical absolute couplings (V in cm^{-1}) used to compute the total coupling and EET rate constant in the fully-optimised dyad **1** reported in Table 1 using different fragment definitions (see Figure S1).

Fragment	BODIPY/ZnP states	V^{coul}	V^{xc}	V^{ovlp}	V^{PCM}	V^{tot}
M0	S_1/S_1	0.2	0.0	0.0	0.1	0.1
	S_1/S_2	5.2	0.0	0.0	3.1	2.2
M1	S_1/S_1	0.1	0.0	0.0	0.1	0.1
	S_1/S_2	8.3	0.0	0.0	4.4	3.9
MC1	S_1/S_1	0.1	0.0	0.0	0.1	0.1
	S_1/S_2	7.4	0.0	0.0	4.0	3.4
MC2	S_1/S_1	0.1	0.0	0.0	0.1	0.1
	S_1/S_2	8.3	0.0	0.0	4.4	3.9
MC3	S_1/S_1	0.1	0.0	0.0	0.0	0.1
	S_1/S_2	5.4	0.0	0.0	3.0	2.4
MC4	S_1/S_1	0.2	0.0	0.0	0.1	0.1
	S_1/S_2	7.9	0.0	0.0	4.3	3.6

S2 Comparison between excitations computed with PBE0 and LC-ωPBE in dyads 2–12

Table S2 Comparison between the transition energy ($\Delta E^{th.}_{abs}$ in eV), oscillator strength (f) and molecular orbital (MO) composition of the first excited states (ES) in **1**–**12** obtained with the PBE0 and LC-ωPBE functional. H and L stand for HOMO and LUMO, respectively. Only the major MO contributions (> 10 %, i.e., CI coefficient > 0.22) are reported here. The nature of the excited states is also given. M, B and CT stand for, Macrocycle, BODIPY and charge transfer states, respectively.

		PBE0				LC-ωPBE			
Dyad	ES	$\Delta E^{th.}_{abs}$	f	MO composition (CI coefficient)	Nature	$\Delta E^{th.}_{abs}$	f	MO composition (CI coefficient)	Nature
1	S_1	2.27	0.223	H→L+1 (0.58) H–1→L+2 (0.38)	M	2.03	0.037	H→L (0.52) H–1→L+1 (0.48)	M
	S_2	2.30	0.030	H→L+2 (0.55) H–1→L+1 (0.43)	M	2.03	0.006	H→L+1 (0.51) H–1→L (-0.49)	M
	S_3	2.68	0.002	H→L (0.70)	CT	2.78	0.656	H–2→L+2 (0.70)	B
	S_4	2.88	0.584	H–2→L (0.70)	B	3.24	3.057	H–1→L+1 (0.52) H←L (-0.47)	M
2	S_1	2.28	0.098	H–1→L+2 (-0.40), H→L+1 (0.58)	M	2.03	0.023	H–1→L+1 (-0.48), H→L (0.53)	M
	S_2	2.29	0.050	H–1→L+1 (0.42), H→L+2 (0.56)	M	2.03	0.011	H–1→L (0.49), H→L+1 (0.52)	M
	S_3	2.66	0.001	H→L (0.71)	CT	2.78	0.648	H–2→L+2 (0.70)	B
	S_4	2.88	0.567	H–2→L (0.70)	B	3.26	2.262	H–1→L+1 (0.52), H→L (0.47)	M
3l	S_1	2.31	0.073	H→L+1 (0.57), H–1→L+2 (-0.42)	M	2.04	0.0143	H–1→L+1 (-0.49), H→L (0.51)	M
	S_2	2.31	0.035	H→L+2 (0.56), H–1→L+1 (0.43)	M	2.04	0.0071	H–1→L (0.49), H→L+1 (0.51)	M
	S_3	2.72	0.000	H→L (0.71)	CT	2.78	0.660	H–2→L+2 (0.70)	B
	S_4	2.89	0.607	H–2→L (0.70)	B	3.29	2.341	H–1→L+1 (0.51), H→L (0.48)	M
3f	S_1	2.30	0.047	H–1→L+2 (0.36), H→L+1 (0.49), H→L+2 (-0.23)	M	2.03	0.012	H–1→L+1 (-0.43), H→L (0.47)	M
	S_2	2.31	0.044	H–1→L+1 (-0.37), H→L+1 (0.27), H→L+2 (0.48)	M	2.04	0.006	H–1→L (0.45), H→L+1 (0.46)	M
	S_3	2.38	0.001	H→L (0.66)	CT	2.75	0.794	H–2→L+2 (0.66)	B
	S_4	2.62	0.019	H–1→L (0.70)	CT	3.28	2.020	H–1→L+1 (0.48), H→L (0.46)	M
	S_5	2.82	0.813	H–2→L (0.70)	B	3.30	1.817	H–1→L (0.48), H→L+1 (-0.46)	M
4	S_1	2.30	0.071	H–1→L+2 (0.42), H→L+1 (0.57)	M	2.03	0.017	H–1→L+1 (0.48), H→L (0.51)	M
	S_2	2.31	0.036	H–1→L+1 (-0.43), H→L+2 (0.56)	M	2.04	0.009	H–1→L (-0.48), H→L+1 (0.51)	M
	S_3	2.62	0.000	H→L (0.71)	CT	2.80	0.645	H–2→L+2 (0.70)	B
	S_4	2.89	0.000	H-1→L (0.71)	CT	3.31	2.241	H–1→L+1 (0.52), H→L (-0.48)	M
	S_5	2.91	0.592	H–2→L (0.70)	B	3.32	1.891	H–1→L (0.51), H→L+1 (0.48)	M
5	S_1	1.94	0.357	H–1→L (-0.36), H→L (0.61)	B, CT	1.94	0.973	H–2→L (0.69)	B
	S_2	1.97	0.581	H–1→L (0.61), H→L (0.36)	B, CT	2.04	0.009	H–1→L+1 (0.25), H–1→L+2 (-0.43), H→L+1 (0.44), H→L+2 (0.26)	M
	S_3	2.16	0.000	H–2→L (0.71)	CT	2.04	0.003	H–1→L+1 (0.43), H–1→L+2 (0.25), H→L+1 (-0.26), H→L+2 (0.44)	M
	S_4	2.31	0.054	H–2→L+2 (-0.42), H→L+1 (0.56)	M	3.29	0.351	H–3→L (0.54)	B
	S_5	2.32	0.026	H–2→L+1 (0.45), H→L+2 (0.54)	M	3.30	1.986	H→L+1 (0.44), H–1→L+2 (0.46), H–3→L (-0.24)	M
6-a	S_1	2.16	0.001	H–3→L (0.31), H→L (0.63)	CT	2.03	0.015	H–1→L+1[a] (-0.34), H→L (0.48), H–1→L+2[a] (0.30)	M
	S_2	2.28	0.059	H–1→L+2 (-0.40), H→L+1 (0.58)	M	2.03	0.013	H–1→L (0.45), H→L+1[a] (0.36), H→L+2[a] (-0.32)	M
	S_3	2.28	0.081	H–1→L+1 (0.40), H→L+2 (0.58),	M	2.77	0.491	H–3→L+1[a] (0.47), H–3→L+2[a](0.51)	B
	S_4	2.42	0.040	H–2→L (0.70)	B[b]	3.28	2.269	H–1→L (0.51), H→L+1[a] (-0.36), H→L+2[a] (0.32)	M
	S_5	2.50	0.000	H-3→L (0.49), H–1→L (0.40), H→L (-0.31)	CT	3.29	2.071	H→L (0.47), H–1→L+1 (0.38), H–1→L+2[a] (-0.34)	M
	S_6	2.62	0.000	H–1→L (0.57), H-3→L (-0.40)	CT	3.92	0.000	H–4→L+1[a] (0.42), H–4→L+2[a] (0.44)	CT
	S_7	2.82	0.376	H–3→L+2 (0.55), H–1→L+1 (-0.26)	M	4.02	0.189	H–2→L+1[a] (0.40), H–2→L+2[a] (0.43)	CT
	S_8	2.86	0.278	H–4→L (0.65)	B	4.08	0.018	H–8→L (0.69)	M

[a] these LUMO orbitals are delocalised on the two fragments
[b] this state corresponds to a CT in the BODIPY unit (from the triphenylamino group to the core of the BODIPY)

Table S3 Follow-up of Table S2

		PBE0				LC-ωPBE			
Dyad	ES	$\Delta E^{th.}_{abs}$	f	MO composition (CI coefficient)	Nature	$\Delta E^{th.}_{abs}$	f	MO composition (CI coefficient)	Nature
6-b	S_1	2.27	0.071	H→L+1 (0.59), H–1→L+2 (-0.38)	M	2.02	0.020	H–1→L+1 (0.43), H→L (0.48), H→L+1 (-0.23)	M
	S_2	2.27	0.089	H→L+2 (0.57), H–1→L+1 (0.39)	M	2.02	0.018	H–1→L (-0.43), H→L (0.23), H→L+1 (0.47)	M
	S_3	2.30	0.000	H→L (0.62)	CT	2.77	0.498	H–2→L+2 (0.69)	B
	S_4	2.61	0.001	H–3→L (0.38), H–2→L (0.34), H–1→L (0.38), H→L (-0.30)	CT	3.27	2.232	H–1→L (0.51), H→L+1 (0.46)	M
	S_5	2.78	0.949	H–2→L (0.63), H–1→L+2 (0.24)	B	3.27	2.091	H→L (-0.46), H–1→L+1 (0.51)	M
7	S_1	2.24	0.167	H–1→L+1 (0.27), H→L (0.61)	M, CT	2.04	0.014	H–1→L+1 (0.46), H→L[a] (0.43), H→L+2[a] (-0.23)	M
	S_2	2.31	0.027	H–1→L (-0.30), H–1→L+2 (0.31), H→L+1 (0.53)	CT, M	2.04	0.010	H–1→L[a] (-0.41), H–1→L+2[a] (0.23), H→L+1 (0.48)	M
	S_3	2.42	0.042	H–1→L+1 (-0.32), H→L (0.34), H→L+2(0.52)	M, CT	2.70	1.449	H–2→L[a] (0.37), H–2→L+2[a] (0.52)	B
	S_4	2.61	0.338	H–1→L (0.62), H–1→L+2 (0.24)	CT, M	3.29	2.100	H–1→L[a] (0.37), H–1→L+1 (0.31), H→L[a] (-0.27), H→L+1 (0.39)	M
	S_5	2.77	0.949	H–2→L (0.58), H–1→L+2 (0.24)	B, M	3.35	1.018	H–1→L[a] (-0.26), H–1→L+1 (0.39) H→L[a] (-0.32), H→L+1 (-0.29)	M
8	S_1	2.31	0.034	H–1→L+2 (0.43), H→L+1 (0.56)	M	2.03	0.009	H–1→L (-0.49), H→L+1 (0.51)	M
	S_2	2.31	0.041	H–1→L+1 (-0.43), H→L+2 (0.55)	M	2.04	0.009	H–1→L+1 (0.9), H→L (0.52)	M
	S_3	2.59	0.000	H→L (0.71)	CT	2.82	0.537	H–2→L+2 (0.69)	B
	S_4	2.82	0.001	H–1→L (0.70)	CT	3.32	1.96	H–1→L (0.43), H–1→L+1 (-0.27), H→L (0.25), H→L+1 (0.42)	M
	S_5	2.91	0.415	H–2→L (0.70)	B	3.32	2.008	H–1→L (0.27), H–1→L+1 (0.44), H→L (-0.41), H→L+1 (0.26)	M
9	S_1	2.24	0.059	H–2→L+1 (0.39), H–1→L (0.58)	M	1.94	0.019	H–1→L+1 (0.47), H→L (0.54)	M
	S_2	2.25	0.056	H–2->L (-0.40), H–1->L+1 (0.57)	M	1.95	0.015	H–1→L (-0.48), H→L+1 (0.53)	M
	S_3	2.45	0.001	H->L (0.71)	CT	2.79	0.553	H–2→L+2 (0.68)	B
	S_4	2.48	0.000	H->L+1 (0.71)	CT	3.24	1.612	H–1→L (0.47), H→L+1 (0.44)	M
	S_5	2.88	0.438	H-> L+3 (0.69)	B	3.25	1.796	H→L (-0.43), H–1→L+1 (0.48)	M
10	S_1	1.96	0.867	H→L (0.70)	M	1.70	0.799	H→L (0.69)	M
	S_2	2.02	0.613	H→L+1 (0.70)	M	1.76	0.634	H→L+1 (0.69)	M
	S_3	2.53	0.002	H→L+2 (0.71)	CT	2.80	0.649	H–1→L+2 (0.69)	B
	S_4	2.59	0.001	H–1→L (0.71)	CT	3.66	0.001	H–8→L (0.26), H–7→L (0.52), H–5→L (0.29)	M
	S_5	2.66	0.000	H–1→L+1 (0.71)	CT	3.70	0.000	H–8→L+1 (0.26), H–7→L+1 (0.52) H–5→L+1 (0.29)	M
	S_6	2.89	0.595	H–1→L+2 (0.70)	B	3.82	0.905	H–2→L (0.39), H→L+3 (-0.38)	CT, M
11	S_1	1.81	1.103	H→L+2 (0.71)	B	2.10	1.213	H→L (0.65)	B
	S_2	1.96	0.001	H→L (0.71)	CT	2.34	0.451	H–1→L+1 (0.68)	M
	S_3	1.97	0.000	H→L+1 (0.71)	CT	2.34	0.475	H–1→L+2 (0.69)	M
	S_4	2.43	0.421	H–2→L (0.70)	M	3.49	2.957	H–2→L (0.55), H→L+4 (0.31)	B
	S_5	2.44	0.439	H–2→L+1 (0.70)	M	3.98	0.058	H–3→L (0.43), H–2→L+4 (-0.29), H→L+8 (0.34)	B
12	S_1	1.59	0.094	H→L (0.49), H–1→L+1 (-0.45)	M	1.32	0.152	H–1→L+1 (-0.4), H→L (0.57)	M
	S_2	1.59	0.062	H→L+1 (0.47), H–1→L (0.47)	M	1.33	0.118	H–1→L (0.44), H→L+1 (0.57)	M
	S_3	2.06	0.465	H–1→L+1(0.51), H→L (0.47)	M	2.36	0.519	H–1→L+1 (0.54), H→L (0.42)	M
	S_4	2.09	0.415	H–1→L (0.50), H→L+1 (0.49)	M	2.40	0.453	H–1→L (0.55), H→L+1 (-0.42)	M
	S_5	2.17	0.000	H–2→L (0.71)	CT	2.56	0.765	H–2→L+2 (0.68)	B
	S_6	2.22	0.000	H–2→L+1 (0.71)	CT	3.03	0.017	H–3→L+1 (0.48), H–1→LUMO+3 (-0.41)	M
	S_7	2.48	0.685	H–2→L+2 (0.71)	B	3.05	0.141	H→L+3 (0.62)	M

[a] these LUMO orbitals are delocalised on the two fragments

S3 Functional and atomic basis set benchmarks

Table S4 Theoretical absolute couplings (V in cm^{-1}) used to compute the total coupling and EET rate constant in in the fully-optimised dyad **1** reported in Tables 4 and 5 using the **MC1** fragment definition (see Figure S1) with different exchange-correlation functionals and atomic basis sets.

Method/6-31+G(d)	BODIPY/ZnP states	V^{coul}	V^{xc}	V^{ovlp}	V^{PCM}	V^{tot}
PBE0	S_1/S_1	0.1	0.0	0.0	0.1	0.1
	S_1/S_2	7.4	0.0	0.0	4.0	3.4
B3LYP	S_1/S_1	0.1	0.0	0.0	0.1	0.1
	S_1/S_2	7.9	0.0	0.0	4.2	3.7
M06-2X	S_1/S_1	0.2	0.0	0.0	0.1	0.1
	S_1/S_2	4.3	0.0	0.0	2.7	1.6
CAM-B3LYP	S_1/S_1	0.2	0.0	0.0	0.1	0.1
	S_1/S_2	3.6	0.0	0.0	2.4	1.2
EOM-CCSD (BODIPY) / PBE0(ZnP)	S_1/S_1	0.1	0.0	0.0	0.1	0.1
	S_1/S_2	6.8	0.0	0.0	3.7	3.1
PBE0/Atomic basis set	BODIPY/ZnP states	V^{coul}	V^{xc}	V^{ovlp}	V^{PCM}	V^{tot}
6-31+G(d)	S_1/S_1	0.1	0.0	0.0	0.1	0.1
	S_1/S_2	7.4	0.0	0.0	4.0	3.4
6-311+G(d)	S_1/S_1	0.1	0.0	0.0	0.1	0.1
	S_1/S_2	6.7	0.0	0.0	3.7	3.1
6-311+G(2d,p)	S_1/S_1	0.1	0.0	0.0	0.1	0.1
	S_1/S_2	6.5	0.0	0.0	3.6	3.0

S4 Rotational analysis in 1

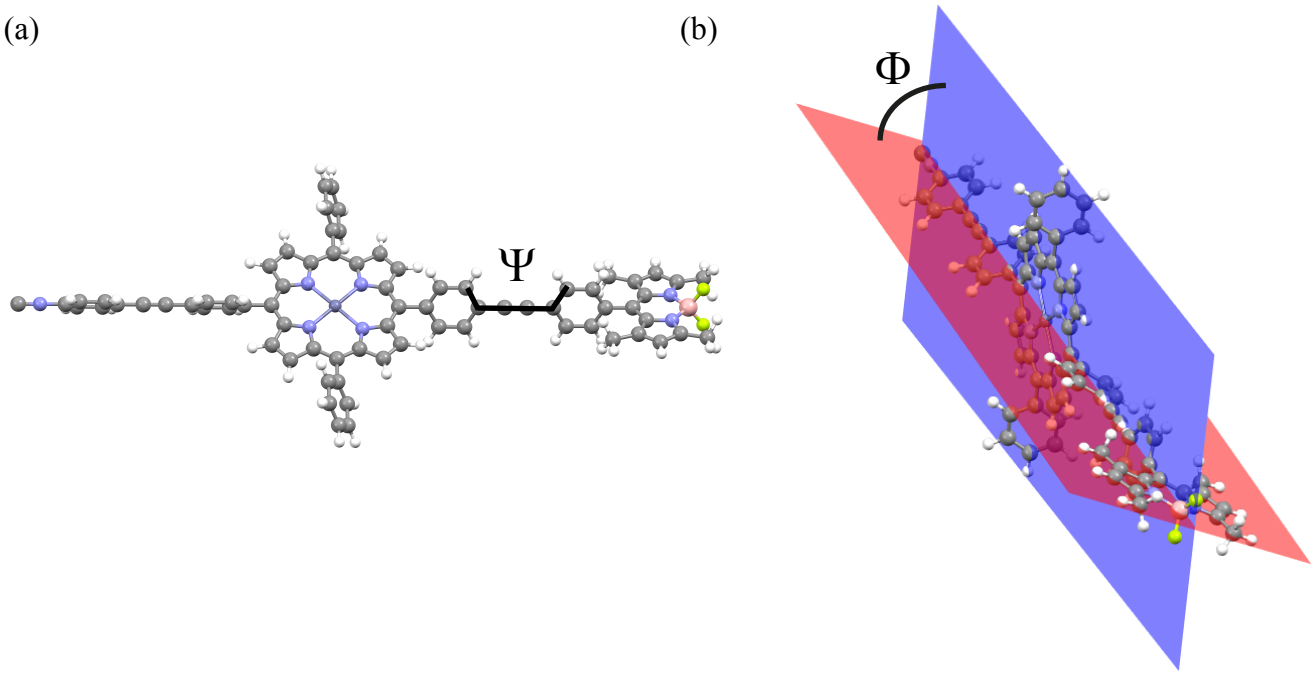

Fig. S2 Representation of the angles (a) Ψ and (b) Φ considered in the rotational analysis. The BODIPY (ZnP) plane is the red (blue) plane.

Table S5 Theoretical absolute total couplings (V^{Whole} in cm^{-1}) in dyad **1** when incrementing by 30° the Ψ dihedral angle between the two *meso* phenyls linked through the ethynyl bridge. The value of the angle Φ between the planes of the BODIPY and ZnP as well as the relative electronic energies ($E_{\mathrm{rel.}}$ in kcal/mol). The angles are given in degrees. Note that the 0° value corresponds to the fully-optimised geometry. The **MC1** fragmentation is applied.

Increment on Ψ	Angle Ψ	Angle Φ	$E_{\mathrm{rel.}}$	V^{Whole}
0	6	22	0.0	3.4
30	36	8	0.3	3.7
60	66	38	0.8	3.1
90	96	68	1.0	1.8
120	126	82	0.7	0.8
150	156	52	0.2	2.2

S5 Orientation of the *meso* phenyl of the ZnP moiety in 1

We have also assessed if the orientation of the *meso* phenyl rings attached to the ZnP moiety has an effect on the EET coupling. We note here that we performed a rigid rotation of the phenyls, the structures have not been re-optimised. It turns out that changing the orientation of the *meso* phenyl rings of the ZnP moiety has no influence on the coupling with the BODIPY unit. Indeed, we obtained a total coupling of 3.4 and 3.5 cm^{-1} for the structures represented in Figure S3b and S3c, respectively.

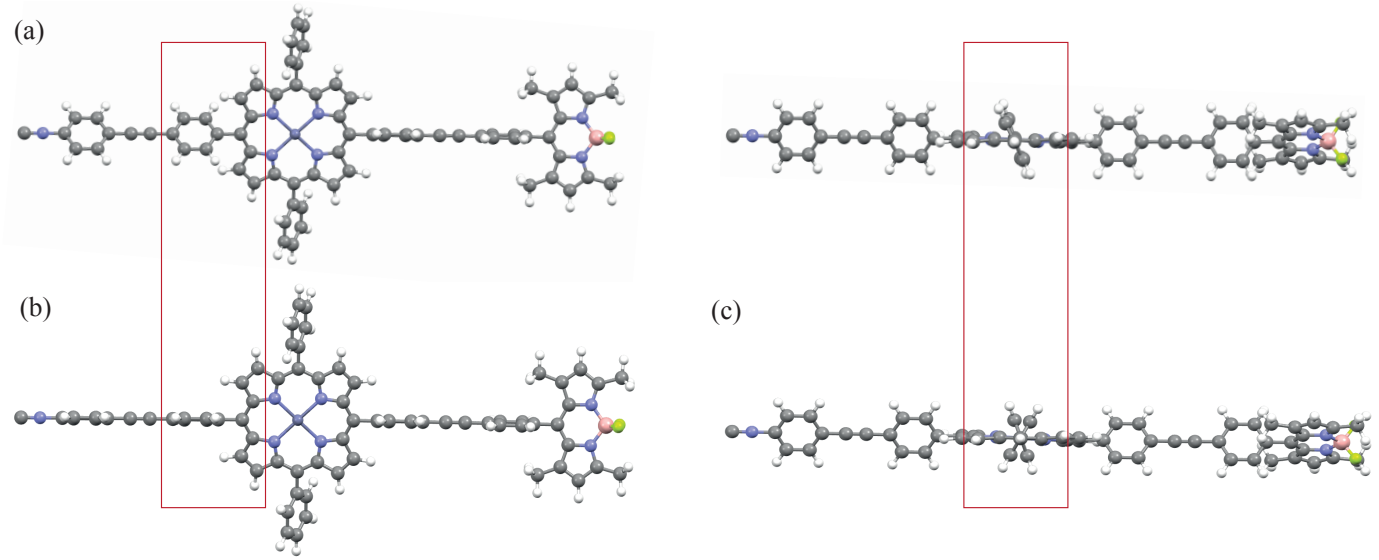

Fig. S3 Representation of (a) **1** in its optimised structure (two views); (b) **1** after rotating the *meso* phenyl bearing the isocyanide ligand and (c) **1** after rotating of one of the two substituent-free *meso* phenyl rings so that all the *meso* phenyl on the porphyrin are arranged in an "helicoidal" manner. The differences between the optimised structure and the two modified ones are highlighted in red squares for the sake of clarity.

S6 Fragmentations used in Table 5 for dyads 2–11

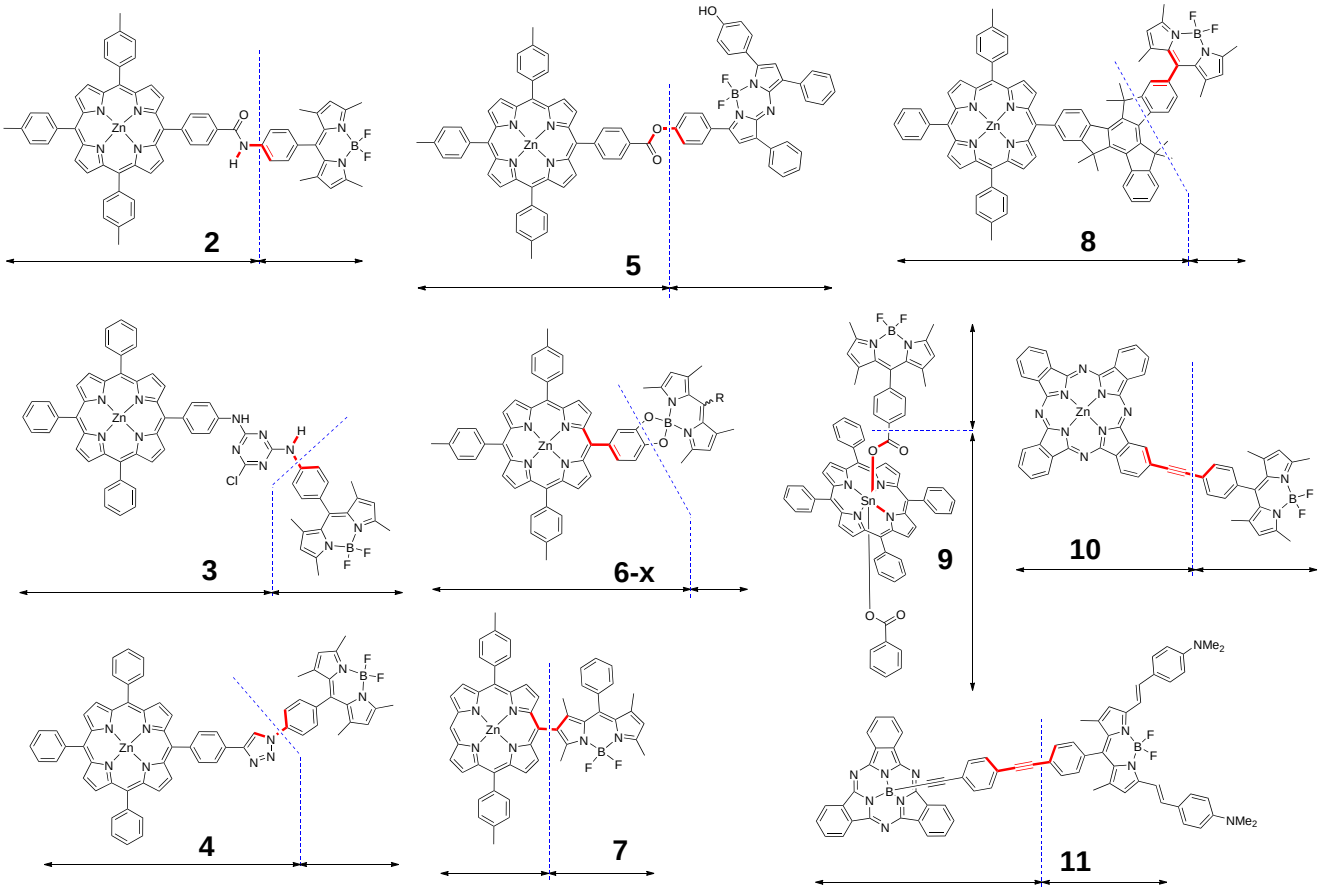

Fig. S4 Representation of the different fragmentation schemes used to compute the coupling values reported in Table 5 in the main text. The dihedral angles Φ considered in the rotational analysis are also displayed in red.

Table S6 Theoretical absolute couplings (V in cm^{-1}) used to compute the total coupling and EET rate constant in the fully-optimised dyads **1**-**11** reported in Table 5 (see Figure S4 for the fragment definition used here).

Dyad	V^{coul}	V^{xc}	V^{ovlp}	V^{PCM}	V^{tot}
1	0.1	0.0	0.0	0.1	0.1
	7.4	0.0	0.0	4.0	3.4
2	0.1	0.0	0.0	0.0	0.1
	11.9	0.0	0.0	6.4	5.4
3l	1.2	0.0	0.0	0.6	0.7
	5.7	0.0	0.0	2.9	2.8
3f	10.3	0.2	0.0	5.1	5.0
	36.2	0.9	0.0	10.7	24.6
4	1.5	0.0	0.0	0.5	1.0
	5.0	0.0	0.0	2.3	2.7
5	74.8	1.1	0.0	34.7	39.0
	5.3	0.0	0.0	3.1	2.2
6-a	19.3	0.0	0.0	11.1	8.2
	0.7	0.1	0.0	1.1	0.3
6-b	27.0	0.1	0.0	15.5	11.6
	4.2	0.1	0.0	1.9	2.2
7	67.9	8.8	0.2	6.8	52.4
	214.2	10.5	0.4	22.7	181.4
8	3.8	0.0	0.0	1.4	2.4
	29.6	0.0	0.0	12.6	17.1
9	86.4	0.8	0.0	39.3	46.3
	25.8	0.4	0.0	13.4	12.8
10	28.7	0.0	0.0	12.4	16.3
	56.1	0.0	0.0	23.0	33.1
11	2.1	0.0	0.0	0.9	1.2
	32.1	0.0	0.0	13.1	19.1

Table S7 Theoretical absolute total couplings (V^{Whole} in cm^{-1}) when incrementing by 30° the Ψ dihedral angle in dyad **2**–**11**. The value of the angle Φ between the planes of the BODIPY and ZnP as well as the relative electronic energies ($E_{\mathrm{rel.}}$ in kcal/mol). The angles are given in degrees. Note that the 0° value corresponds to the fully-optimised geometry. The **MC1** fragmentation is applied.

Dyad	Increment on Ψ	Angle Ψ	Angle Φ	$E_{\mathrm{rel.}}$	V^{Whole}	Dyad	Increment on Ψ	Angle Ψ	Angle Φ	$E_{\mathrm{rel.}}$	V^{Whole}
2	0	-1	15	0.0	5.4	**6-b**	0	69	37	0.3	11.8
	30	29	35	1.0	4.9		30	99	34	0.4	14.1
	60	59	57	3.1	4.3		60	129	46	0.0	14.5
	90	89	83	4.5	4.3		90	159	66	6.4	10.0
	120	119	54	3.0	4.0		120	-171	83	23.5	24.8
	150	149	31	1.0	4.8		150	-141	53	3.2	5.7
3l	0	0	39	0.0	2.9	**7**	0	-68	68	0.0	188.9
	30	30	29	0.7	3.6		30	-38	49	3.4	207.4
	60	60	45	2.2	4.5		60	-8	36	16.0	244.7
	90	90	65	3.3	6.4		90	22	24	37.3	291.9
	120	120	82	2.2	3.3		120[a]	52	—	—	—
	150	150	60	0.7	2.0		150	82	81	0.4	183.1
3f	0	-24	14	7.4	25.1	**8**	0	83	65	0.0	17.2
	30	6	23	8.8	22.7		30	113	68	0.5	16.1
	60	36	88	9.7	10.9		60	143	78	5.7	13.8
	90	66	89	4.9	9.3		90	173	88	20.2	11.2
	120[a]	96	—	—	—		120	-157	56	18.9	7.0
	150	126	40	0.0	21.4		150	-127	71	2.1	15.5
4	0	-30	59	0.0	2.9	**9**	0	9	62	1.1	48.0
	30	0	32	0.5	4.5		30	39	70	0.6	73.3
	60	30	23	0.0	4.9		60	69	50	0.0	76.7
	90	60	24	1.1	4.9		90	99	64	1.3	47.7
	120	90	70	2.6	2.2		120	129	72	1.9	52.7
	150	120	83	1.2	1.8		150	159	50	0.2	73.3
5	0	7	32	0.8	39.0	**10**	0	-9	75	0.0	11.7
	30	37	20	0.3	40.9		30	21	74	0.1	12.2
	60	67	37	0.4	41.7		60	51	44	0.6	33.0
	90	97	66	0.5	42.7		90	81	15	1.1	45.3
	120	127	83	0.0	44.5		120	111	18	0.9	44.4
	150	157	55	0.5	45.9		150	141	45	0.4	32.3
6-a	0	68	35	0.4	8.2	**11**	0	-2	88	0.0	19.1
	30	98	35	0.4	9.5		30	28	89	0.3	19.0
	60	128	47	0.0	11.3		60	58	89	0.8	18.4
	90	158	67	6.3	8.5		90	88	87	1.1	18.2
	120	-172	86	23.3	14.3		120	118	87	0.9	18.5
	150	-142	53	3.6	2.2		150	148	86	0.3	18.9

[a] for those angles, we obtained a steric clash between the atoms of the donor and acceptor moieties.

S7 Fragment definition in dyad 2

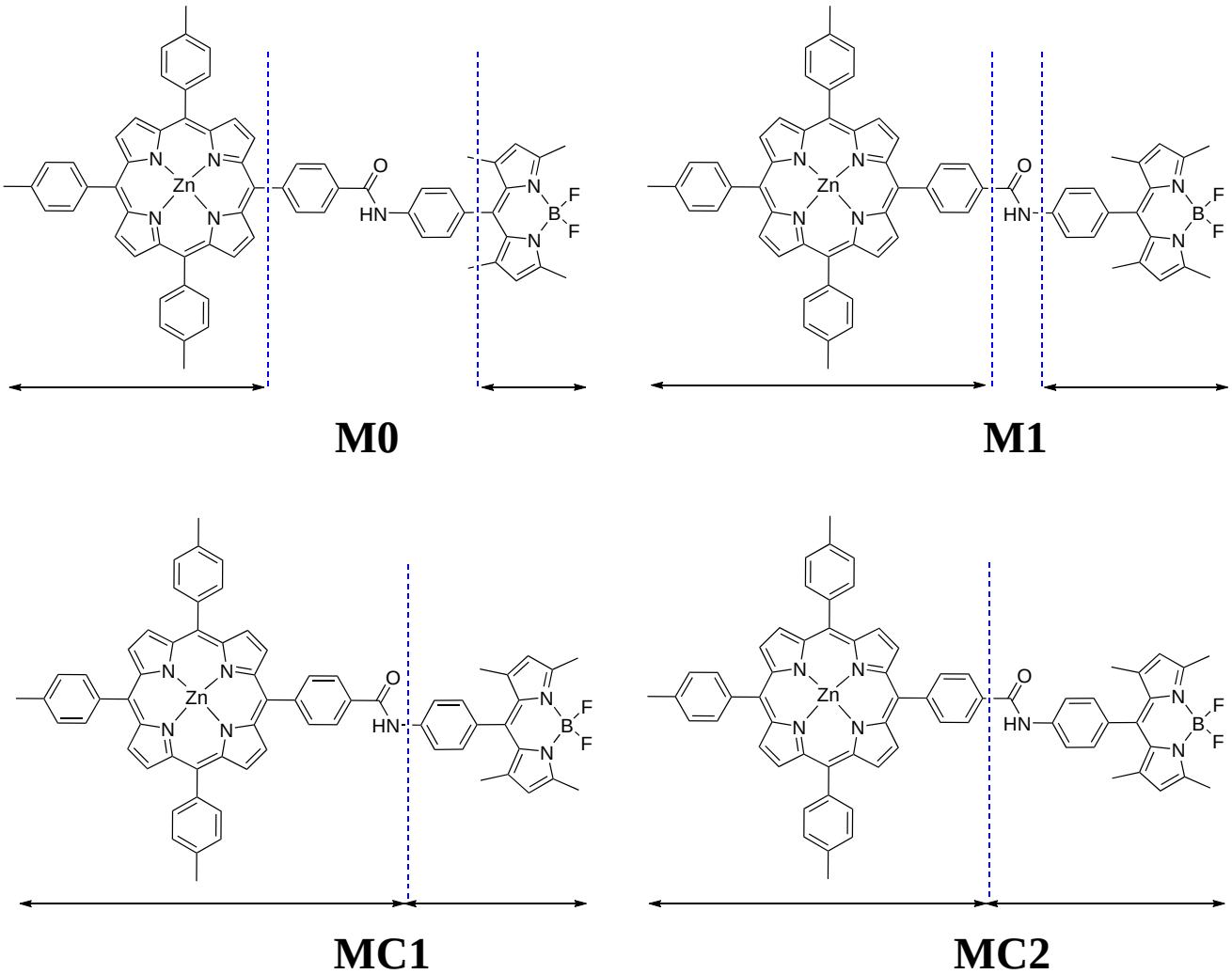

Fig. S5 Representation of the different fragmentation schemes considered in dyad **2**.

Table S8 Calculated transition energies ($\Delta E^{th.}_{abs}$ in eV) and oscillator strengths (f) of the excited-states of the different fragments involved in the electronic coupling in **2** (see Figure S5). Theoretical absolute couplings (V in cm^{-1}) and EET rate constant ($k^{th.}$ in s^{-1}) computed on the fully-optimised structure for each fragmentation scheme are also given.

Fragmentation scheme	BODIPY fragment		ZnP fragment		EET Coupling						
	$\Delta E^{th.}_{abs}$	f	$\Delta E^{th.}_{abs}$	f	V^{coul}	V^{xc}	V^{ovlp}	V^{PCM}	V^{tot}	V^{Whole}	$k^{th.}$
M0	2.83	0.684	2.33	0.022	1.3	0.0	0.0	0.7	0.5	4.5	5.8×10^{9}
			2.33	0.043	10.2	0.0	0.0	5.7	4.5		
M1	2.88	0.652	2.29	0.064	2.0	0.0	0.0	1.0	1.0	6.4	1.1×10^{10}
			2.29	0.061	13.4	0.0	0.0	7.2	6.3		
MC1	2.88	0.652	2.28	0.080	0.1	0.0	0.0	0.0	0.1	5.4	8.4×10^{9}
			2.30	0.052	11.9	0.0	0.0	6.4	5.4		
MC2	2.87	0.649	2.29	0.064	1.9	0.0	0.0	1.0	0.9	6.3	1.1×10^{10}
			2.29	0.061	13.4	0.0	0.0	7.2	6.3		

S8 Fragment definition in dyad 3

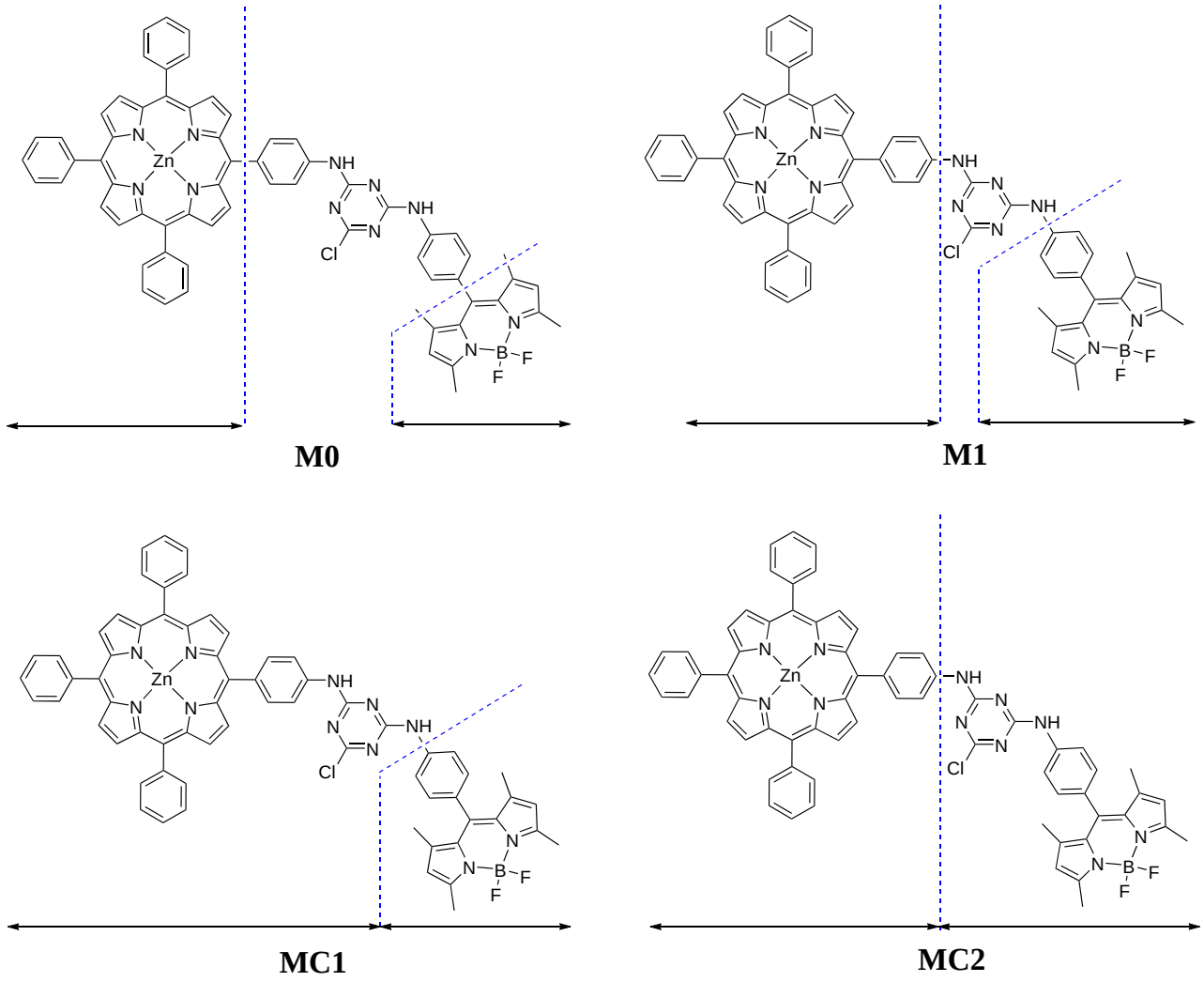

Fig. S6 Representation of the different fragmentation schemes considered in dyad **3**.

Table S9 Calculated transition energies ($\Delta E^{th.}_{abs}$ in eV) and oscillator strengths (f) of the excited-states of the different fragments involved in the electronic coupling (see Figure S6) in the two key conformers of **3**, namely **3l** ("linear" conformation) and **3f** ("folded" conformation), see Figure 5 in the main text. Theoretical absolute couplings (V in cm^{-1}) and EET rate constant ($k^{th.}$ in s^{-1}) computed on the fully-optimised structure for each fragmentation scheme are also given.

Conformer	Fragmentation	BODIPY fragment		ZnP fragment		EET Coupling						
3l$^{\diamond}$	scheme	$\Delta E^{th.}_{abs}$	f	$\Delta E^{th.}_{abs}$	f	V^{coul}	V^{xc}	V^{ovlp}	V^{PCM}	V^{tot}	V^{Whole}	$k^{th.}$
	M0	2.83	0.681	2.35	0.020	3.8	0.0	0.0	2.1	1.7	1.8	8.8×10^{8}
				2.35	0.010	0.6	0.0	0.0	0.2	0.4		
	M1	2.88	0.650	2.31	0.040	1.4	0.0	0.0	0.6	0.7	2.7	2.1×10^{9}
				2.32	0.033	5.3	0.0	0.0	2.7	2.6		
	MC1	2.88	0.650	2.31	0.064	1.2	0.0	0.0	0.6	0.7	2.9	2.4×10^{9}
				2.31	0.036	5.7	0.0	0.0	2.9	2.8		
	MC2	2.88	0.644	2.31	0.040	1.3	0.0	0.0	0.6	0.7	2.7	2.0×10^{9}
				2.32	0.0.33	5.3	0.0	0.0	2.7	2.6		
3f$^{\diamond}$	Fragmentation	BODIPY fragment		ZnP fragment		EET Coupling						
	scheme	$\Delta E^{th.}_{abs}$	f	$\Delta E^{th.}_{abs}$	f	V^{coul}	V^{xc}	V^{ovlp}	V^{PCM}	V^{tot}	V^{Whole}	$k^{th.}$
	M0	2.84	0.671	2.35	0.021	7.8	0.8	0.0	0.2	7.2	16.1	7.4×10^{10}
				2.35	0.011	22.6	0.0	0.0	8.2	14.4		
	M1	2.85	0.610	2.31	0.036	5.4	0.1	0.0	2.0	3.4	22.8	1.5×10^{11}
				2.31	0.036	32.9	0.9	0.0	9.5	22.5		
	MC1	2.85	0.610	2.31	0.057	10.3	0.2	0.0	5.1	5.0	25.1	1.8×10^{11}
				2.31	0.040	36.2	0.9	0.0	10.7	24.6		
	MC2	2.85	0.595	2.31	0.036	1.5	0.2	0.0	0.6	1.0	23.2	1.5×10^{11}
				2.31	0.036	34.2	0.9	0.0	10.2	23.1		
3f*	Fragmentation	BODIPY fragment		ZnP fragment		EET Coupling						
	scheme	$\Delta E^{th.}_{abs}$	f	$\Delta E^{th.}_{abs}$	f	V^{coul}	V^{xc}	V^{ovlp}	V^{PCM}	V^{tot}	V^{Whole}	$k^{th.}$
	MC1	2.88	0.601	2.29	0.072	44.7	0.6	0.0	20.0	24.2	80.1	1.8×10^{12}
				2.30	0.034	130.9	0.7	0.0	55.2	76.4		

$\diamond$ optimised at the PBE0-D3^{BJ} level
* optimised at the PBE0-D3 level

S9 Evaluation of the experimental EET rate constant in 4

For dyad **4**, the EET rate constant has not been experimentally reported. However, the EET efficiency (η) has been calculated to be 95.8 %, using the fluorescence intensity of the donor (BODIPY unit) in the presence (I_D) or in absence (I_D°) of the acceptor(ZnP) part, according to the following equation:

$$\eta = 1 - \frac{I_D}{I_D^\circ} \tag{S1}$$

As the lifetime of the unquenched donor (τ_D°) has been experimentally measured, and considering that the EET efficiency can be written using the fluorescence yield of the unquenched/quenched donor (Φ_D°/Φ_D):

$$\eta = 1 - \frac{\Phi_D}{\Phi_D^\circ}, \quad \text{with} \quad \Phi_D^\circ = \frac{k_r}{k_r + k_{nr}} = \frac{k_r}{k^\circ} \quad \text{and} \quad \Phi_D = \frac{k_r}{k_r + k_{nr} + k_{EET}} \tag{S2}$$

One can therefore estimate the EET rate constant (k_{EET}) value according to:

$$k_{EET} = \frac{1}{\tau_D^\circ}\left(\frac{\eta}{1-\eta}\right) \tag{S3}$$

with k_r, k_{nr} corresponding to the radiative, non-radiative and EET rate constants, respectively.

S10 Fragment definition in dyad 4

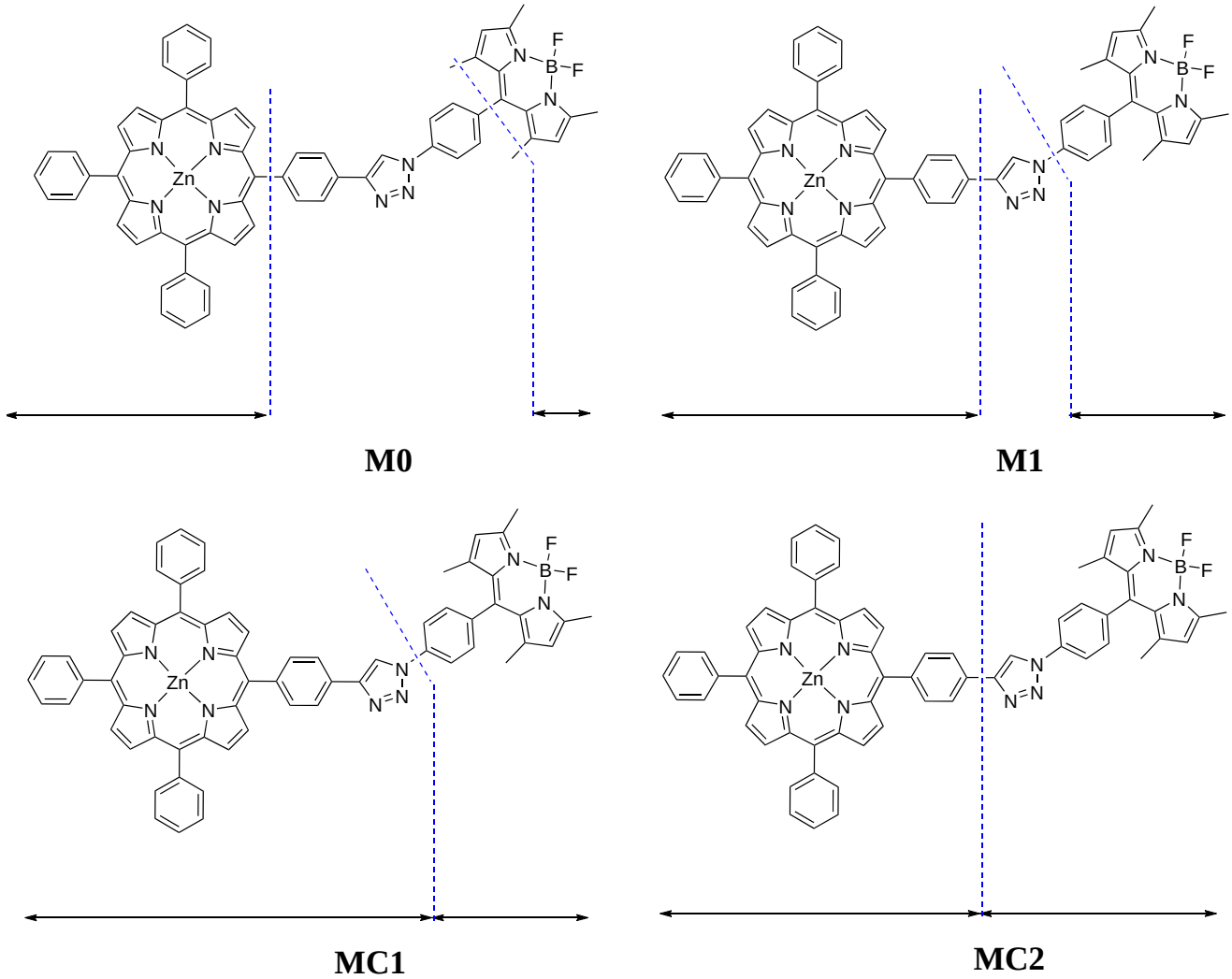

Fig. S7 Representation of the different fragmentation schemes considered in dyad **4**.

Table S10 Calculated transition energies ($\Delta E^{th.}_{abs}$ in eV) and oscillator strengths (f) of the excited-states of the different fragments involved in the electronic coupling in **4** (see Figure S7). Theoretical absolute couplings (V in cm^{-1}) and EET rate constant ($k^{th.}$ in s^{-1}) computed on the fully-optimised structure for each fragmentation scheme are also given.

Fragmentation	BODIPY fragment		ZnP fragment		EET Coupling						
scheme	$\Delta E^{th.}_{abs}$	f	$\Delta E^{th.}_{abs}$	f	V^{coul}	V^{xc}	V^{ovlp}	V^{PCM}	V^{tot}	V^{Whole}	$k^{th.}$
M0	2.86	0.659	2.35	0.017	1.4	0.0	0.0	0.8	0.5	2.0	1.2×10^{9}
			2.35	0.018	3.7	0.0	0.0	1.7	2.0		
M1	2.91	0.627	2.31	0.042	1.7	0.0	0.0	0.6	1.1	3.0	2.6×10^{9}
			2.31	0.038	5.2	0.0	0.0	2.3	2.8		
MC1	2.91	0.627	2.30	0.061	1.5	0.0	0.0	0.5	1.0	2.9	2.4×10^{9}
			2.31	0.037	5.0	0.0	0.0	2.3	2.7		
MC2	2.90	0.621	2.31	0.042	1.3	0.0	0.0	0.5	0.9	2.9	2.5×109
			2.31	0.038	5.1	0.0	0.0	2.3	2.8		

S11 Fragment definition in dyad 5

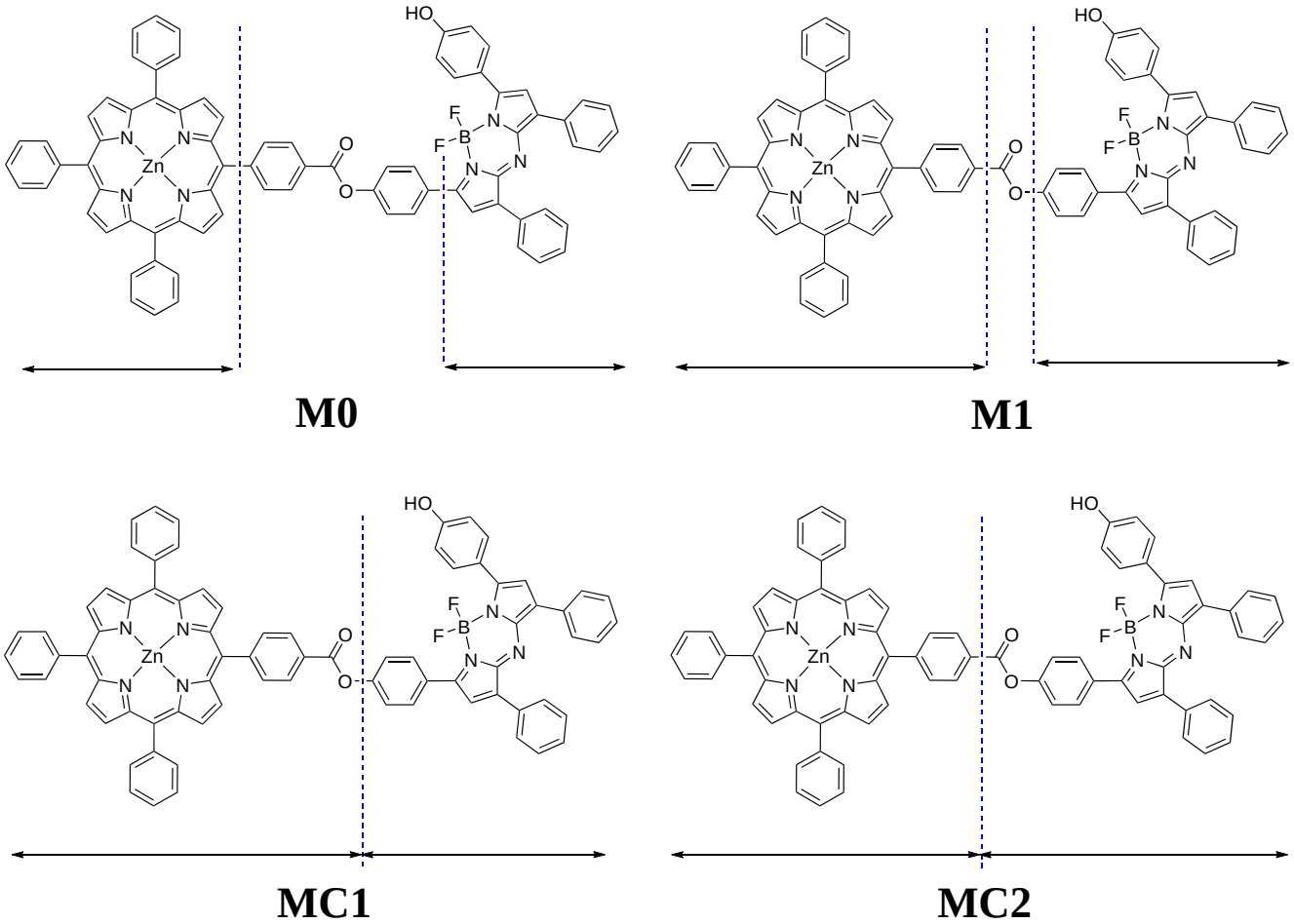

Fig. S8 Representation of the different fragmentation schemes considered in dyad **5**.

Table S11 Calculated transition energies ($\Delta E^{th.}_{abs}$ in eV) and oscillator strengths (f) of the excited-states of the different fragments involved in the electronic coupling in **5** (see Figure S8). Theoretical absolute couplings (V in cm^{-1}) and EET rate constant ($k^{th.}$ in s^{-1}) computed on the fully-optimised structure for each fragmentation scheme are also given.

Fragmentation	BODIPY fragment		ZnP fragment		EET Coupling						
scheme	$\Delta E^{th.}_{abs}$	f	$\Delta E^{th.}_{abs}$	f	V^{coul}	V^{xc}	V^{ovlp}	V^{PCM}	V^{tot}	V^{Whole}	$k^{th.}$
M0	2.15	0.897	2.35	0.020	8.2	0.0	0.0	4.7	3.5	3.5	3.6×10^{9}
			2.35	0.009	1.8	0.0	0.0	1.3	0.6		
M1	1.99	0.865	2.32	0.034	42.2	0.3	0.0	21.5	20.4	25.6	1.9×10^{11}
			2.32	0.034	31.8	0.3	0.0	15.9	15.5		
MC1	1.99	0.865	2.31	0.047	74.8	1.1	0.0	34.7	39.0	39.0	4.3×10^{11}
			2.32	0.027	5.3	0.0	0.0	3.1	2.2		
MC2	1.97	0.863	2.32	0.034	52.1	0.8	0.0	24.5	26.9	35.9	3.6×10^{11}
			2.32	0.034	44.6	0.9	0.0	20.0	23.8		

S12 Additional EET data in 6-x dyads

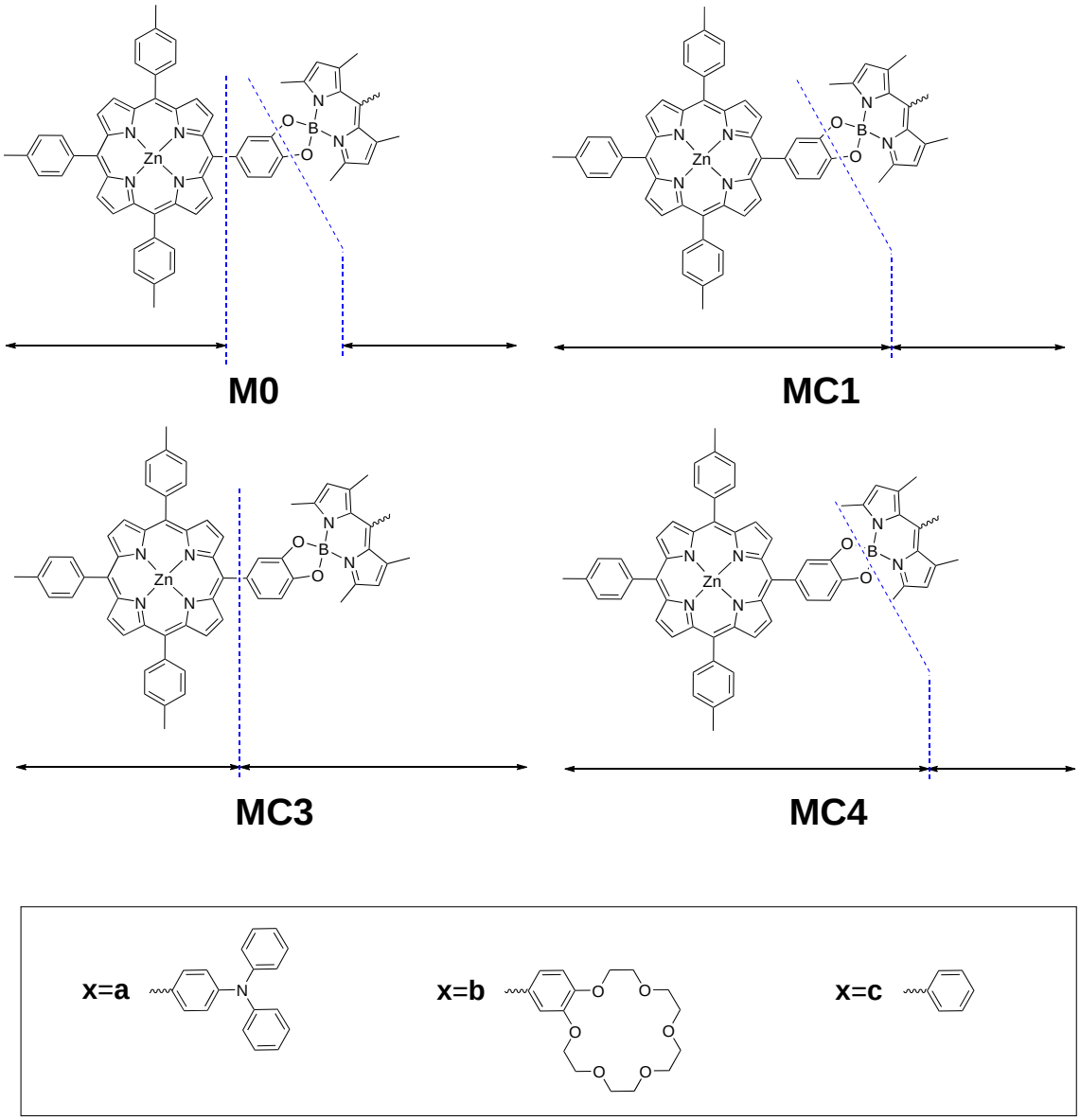

Fig. S9 Representation of the different fragmentation schemes considered in dyad **6-x**.

Table S12 Calculated transition energies ($\Delta E^{th.}_{abs}$ in eV) and oscillator strengths (f) of the excited-states of the different fragments involved in the electronic coupling in **6-x** (see Figure S9). Theoretical absolute couplings (V in cm^{-1}) and EET rate constant ($k^{th.}$ in s^{-1}) computed on the fully-optimised structure for each fragmentation scheme are also given. We note that the solvent specified has been used for both optimising and computing the EET coupling.

Dyad	Solvent	Fragment	BODIPY fragment		ZnP fragment		EET Coupling						
			$\Delta E^{th.}_{abs}$	f	$\Delta E^{th.}_{abs}$	f	V^{coul}	V^{xc}	V^{ovlp}	V^{PCM}	V^{tot}	V^{Whole}	$k^{th.}$
6-a	Toluene	**M0**	2.86	0.564	2.34	0.031	0.5	0.1	0.0	2.9	2.3	3.1	3.7×10^{9}
					2.34	0.019	4.7	0.0	0.0	2.7	2.1		
		MC1	2.86	0.546	2.31	0.050	19.3	0.0	0.0	11.1	8.2	8.2	2.5×10^{10}
					2.31	0.046	0.7	0.1	0.0	1.1	0.3		
		MC3	2.86	0.556	2.34	0.031	3.7	0.1	0.0	3.7	0.1	2.8	3.0×10^{9}
					2.34	0.019	5.5	0.2	0.0	2.9	2.8		
		MC4	2.95	0.622	2.30	0.052	10.2	0.0	0.0	5.2	5.0	7.7	2.3×10^{10}
					2.30	0.048	15.5	0.1	0.0	9.6	5.9		
Dyad	Solvent	Fragment	BODIPY fragment		ZnP fragment		EET Coupling						
			$\Delta E^{th.}_{abs}$	f	$\Delta E^{th.}_{abs}$	f	V^{coul}	V^{xc}	V^{ovlp}	V^{PCM}	V^{tot}	V^{Whole}	$k^{th.}$
6-a	Benzonitrile	**M0**	2.86	0.570	2.33	0.029	2.5	0.0	0.0	3.1	0.6	3.6	5.0×10^{9}
					2.33	0.038	10.5	0.1	0.0	7.0	3.6		
		MC1	2.86	0.570	2.29	0.064	25.2	0.1	0.0	14.5	10.8	11.7	5.2×10^{10}
					2.29	0.060	9.7	0.0	0.0	5.1	4.6		
		MC3	2.86	0.557	2.33	0.029	4.4	0.0	0.0	3.5	0.9	5.0	9.6×10^{9}
					2.33	0.038	12.0	0.3	0.0	7.4	4.9		
		MC4	2.95	0.627	2.29	0.066	9.4	0.1	0.0	4.9	4.6	11.0	4.6×10^{10}
					2.29	0.062	24.1	0.1	0.0	14.1	10.0		
Dyad	Solvent	Fragment	BODIPY fragment		ZnP fragment		EET Coupling						
			$\Delta E^{th.}_{abs}$	f	$\Delta E^{th.}_{abs}$	f	V^{coul}	V^{xc}	V^{ovlp}	V^{PCM}	V^{tot}	V^{Whole}	$k^{th.}$
6-b	Benzonitrile	**M0**	2.86	0.575	2.33	0.034	5.7	0.1	0.0	5.1	0.6	3.8	5.5×10^{9}
					2.33	0.033	9.9	0.1	0.0	6.3	3.8		
		MC1	2.86	0.575	2.29	0.064	27.0	0.1	0.0	15.5	11.6	11.8	5.3×10^{9}
					2.29	0.056	4.2	0.1	0.0	1.9	2.2		
		MC3	2.86	0.564	2.33	0.034	8.0	0.1	0.0	5.6	2.4	5.2	1.1×10^{10}
					2.33	0.033	10.9	0.3	0.0	6.5	4.7		
		MC4	2.96	0.646	2.29	0.062	9.1	0.0	0.0	4.9	4.2	10.9	4.5×10^{9}
					2.29	0.062	24.4	0.1	0.0	14.3	10.0		
Dyad	Solvent	Fragment	BODIPY fragment		ZnP fragment		EET Coupling						
			$\Delta E^{th.}_{abs}$	f	$\Delta E^{th.}_{abs}$	f	V^{coul}	V^{xc}	V^{ovlp}	V^{PCM}	V^{tot}	V^{Whole}	$k^{th.}$
6-c	Benzonitrile	**M0**	2.87	0.601	2.33	0.030	3.1	0.0	0.0	3.5	0.4	3.7	5.3×10^{9}
					2.33	0.038	10.7	0.1	0.0	7.1	3.7		
		MC1	2.87	0.601	2.29	0.064	25.5	0.0	0.0	14.8	10.8	11.8	5.3×10^{10}
					2.29	0.059	10.1	0.0	0.0	5.3	4.7		
		MC3	2.87	0.590	2.33	0.030	5.0	0.0	0.0	4.0	1.0	5.2	1.4×10^{10}
					2.33	0.038	12.3	0.2	0.0	7.5	5.1		
		MC4	2.96	0.669	2.29	0.065	8.9	0.1	0.0	4.6	4.3	11.0	4.6×10^{10}
					2.29	0.062	24.7	0.1	0.0	14.5	10.1		

S13 Fragment definition in dyad 8

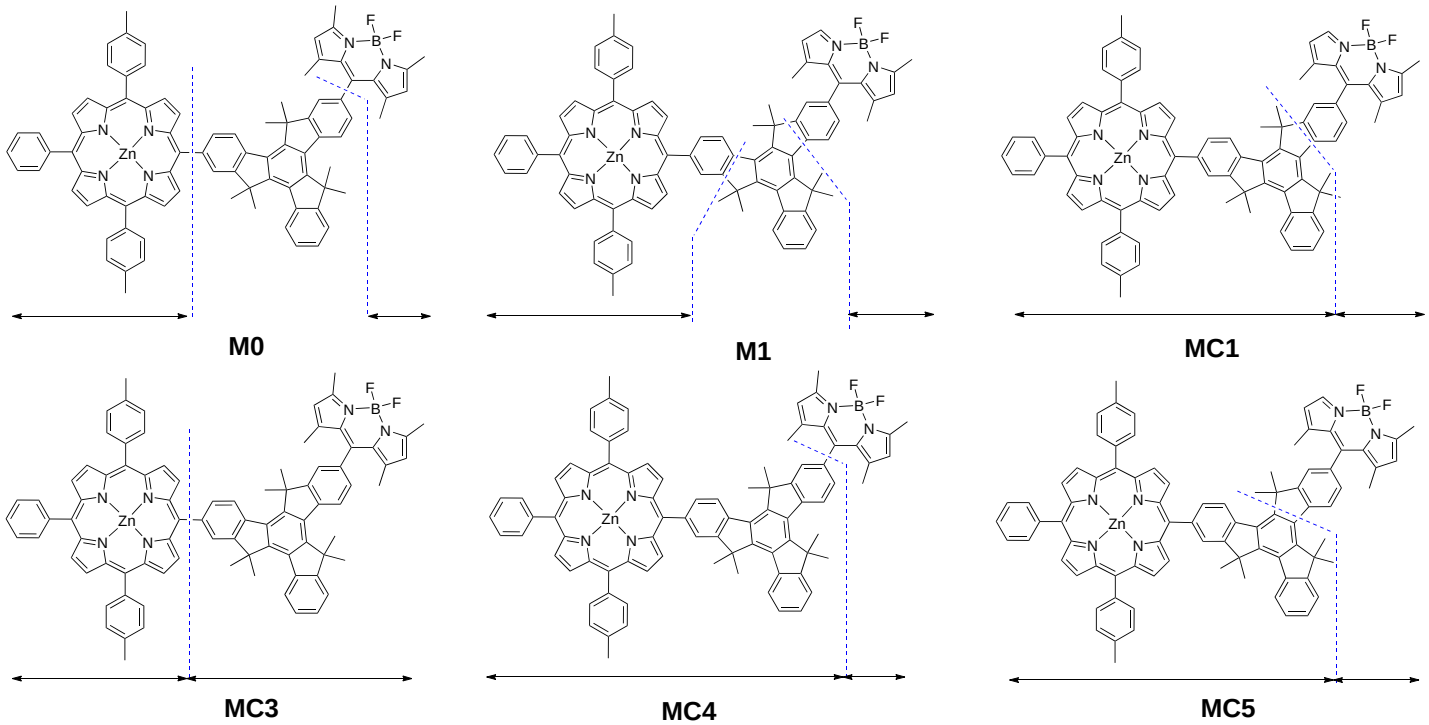

Fig. S10 Representation of the different fragmentation schemes considered in dyad **8**.

Table S13 Calculated transition energies ($\Delta E^{th.}_{abs}$ in eV) and oscillator strengths (f) of the excited-states of the different fragments involved in the electronic coupling in **8** (see Figure S10). Theoretical absolute couplings (V in cm^{-1}) and EET rate constant ($k^{th.}$ in s^{-1}) computed on the fully-optimised structure for each fragmentation scheme are also given.

Fragmentation	BODIPY fragment		ZnP fragment		EET Coupling						
scheme	$\Delta E^{th.}_{abs}$	f	$\Delta E^{th.}_{abs}$	f	V^{coul}	V^{xc}	V^{ovlp}	V^{PCM}	V^{tot}	V^{Whole}	$k^{th.}$
M0	2.86	0.655	2.33	0.025	18.4	0.0	0.0	7.8	10.6	16.7	5.1×10^{10}
			2.34	0.030	22.7	0.0	0.0	9.8	12.9		
M1	2.91	0.618	2.31	0.033	15.1	0.0	0.0	6.3	8.9	18.5	6.2×10^{10}
			2.31	0.043	28.2	0.0	0.0	12.0	16.2		
MC1	2.91	0.618	2.31	0.035	3.8	0.0	0.0	1.4	2.4	17.2	5.4×10^{10}
			2.31	0.043	29.6	0.0	0.0	12.6	17.1		
MC3	2.91	0.583	2.33	0.025	17.7	0.0	0.0	7.4	10.3	15.9	4.6×10^{10}
			2.34	0.030	21.4	0.0	0.0	9.2	12.1		
MC4	2.86	0.655	2.31	0.034	3.8	0.0	0.0	1.5	2.4	17.2	5.4×10^{10}
			2.31	0.043	29.7	0.0	0.0	12.7	17.0		
MC5	2.91	0.607	2.31	0.035	3.7	0.0	0.0	1.4	2.3	17.2	5.4×10^{10}
			2.31	0.043	29.6	0.0	0.0	12.5	17.0		

S14 Fragment definition in dyad 9

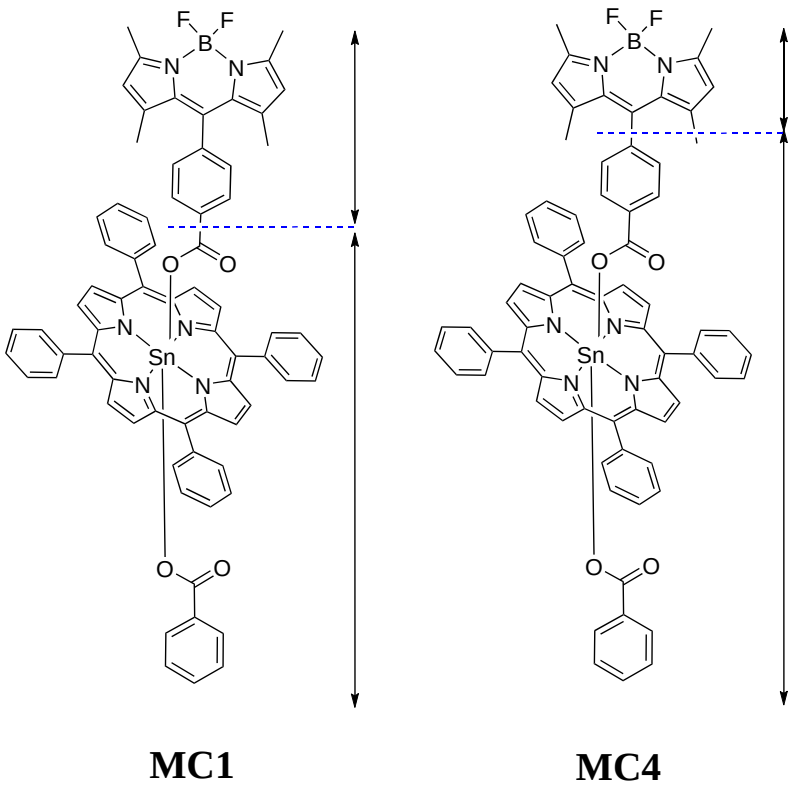

Fig. S11 Representation of the different fragmentation schemes considered in dyad **9**.

Table S14 Calculated transition energies ($\Delta E^{th.}_{abs}$ in eV) and oscillator strengths (f) of the excited-states of the different fragments involved in the electronic coupling in **5** (see Figure S11). Theoretical absolute couplings (V in cm^{-1}) and EET rate constant ($k^{th.}$ in s^{-1}) computed on the fully-optimised structure for each fragmentation scheme are also given.

Fragmentation scheme	BODIPY fragment		Porphyrin fragment		EET Coupling						
	$\Delta E^{th.}_{abs}$	f	$\Delta E^{th.}_{abs}$	f	V^{coul}	V^{xc}	V^{ovlp}	V^{PCM}	V^{tot}	V^{Whole}	$k^{th.}$
MC1	2.83	0.675	2.24	0.062	76.9	0.6	0.0	35.1	41.2	46.5	3.0×10^{11}
			2.25	0.058	42.0	0.4	0.0	20.8	21.6		
MC4	2.89	0.644	2.24	0.065	86.4	0.8	0.0	39.3	46.3	48.0	3.3×10^{11}
			2.25	0.055	25.8	0.4	0.0	13.4	12.8		

S15 Fragment definition in dyad 10

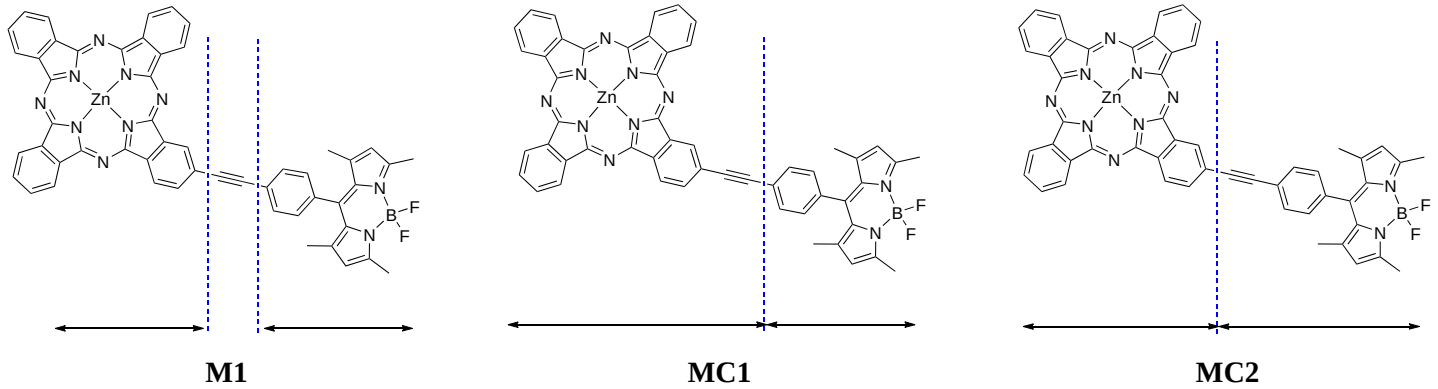

Fig. S12 Representation of the different fragmentation schemes considered in dyad **10**.

Table S15 Calculated transition energies ($\Delta E^{th.}_{abs}$ in eV) and oscillator strengths (f) of the excited-states of the different fragments involved in the electronic coupling in **10** (see Figure S12). Theoretical absolute couplings (V in cm^{-1}) and EET rate constant ($k^{th.}$ in s^{-1}) computed on the fully-optimised structure for each fragmentation scheme are also given.

Fragmentation scheme	BODIPY fragment		Phthalocyanine fragment		EET Coupling						
	$\Delta E^{th.}_{abs}$	f	$\Delta E^{th.}_{abs}$	f	V^{coul}	V^{xc}	V^{ovlp}	V^{PCM}	V^{tot}	V^{Whole}	$k^{th.}$
M1	2.91	0.622	2.01	0.638	11.0	0.0	0.0	4.7	6.3	11.7	2.1×10^{9}
			2.02	0.636	16.7	0.0	0.0	6.9	9.8		
MC1	2.91	0.622	1.98	0.725	8.9	0.0	0.0	3.8	5.1	11.7	2.1×10^{9}
			2.02	0.622	18.0	0.0	0.0	7.4	10.6		
MC2	2.89	0.617	2.01	0.638	11.0	0.0	0.0	4.7	6.4	11.7	2.1×10^{9}
			2.02	0.636	16.6	0.0	0.0	6.8	9.8		

S16 Fragment definition in dyad 11

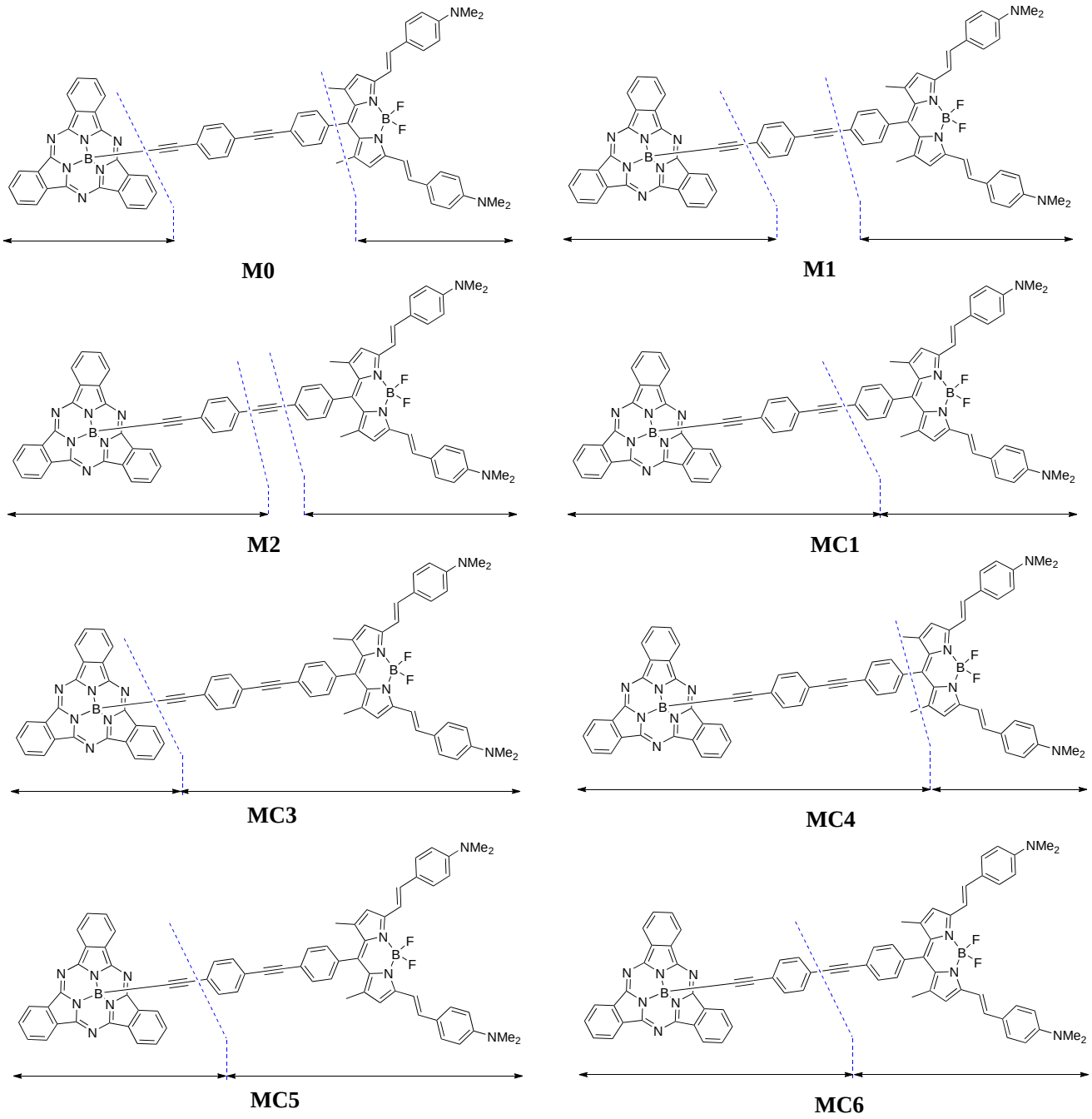

Fig. S13 Representation of the different fragmentation schemes considered in dyad **11**.

Table S16 Calculated transition energies ($\Delta E_{abs}^{th.}$ in eV) and oscillator strengths (f) of the excited-states of the different fragments involved in the electronic coupling in **11** (see Figure S13). Theoretical absolute couplings (V in cm^{-1}) and EET rate constant ($k^{th.}$ in s^{-1}) computed on the fully-optimised structure for each fragmentation scheme are also given.

Fragmentation	BODIPY fragment		Subphthalocyanine fragment		EET Coupling						
scheme	$\Delta E_{abs}^{th.}$	f	$\Delta E_{abs}^{th.}$	f	V^{coul}	V^{xc}	V^{ovlp}	V^{PCM}	V^{tot}	V^{Whole}	$k^{th.}$
M0	1.78	1.145	2.45	0.457	28.4	0.0	0.0	11.3	17.1	21.2	4.5×10^{10}
			2.45	0.457	20.7	0.0	0.0	8.2	12.5		
M1	1.82	1.125	2.44	0.446	1.7	0.0	0.0	0.7	1.0	19.8	3.9×10^{10}
			2.44	0.446	33.1	0.0	0.0	13.3	19.7		
M2	1.82	1.125	2.44	0.433	2.1	0.0	0.0	0.9	1.2	19.2	3.7×10^{10}
			2.44	0.441	32.3	0.0	0.0	13.1	19.2		
MC1	1.82	1.125	2.43	0.427	2.1	0.0	0.0	0.9	1.2	19.1	3.6×10^{10}
			2.44	0.440	32.1	0.0	0.0	13.1	19.1		
MC3	1.81	1.118	2.45	0.457	26.1	0.0	0.0	10.6	15.5	19.1	3.6×10^{10}
			2.45	0.457	18.9	0.0	0.0	7.7	11.2		
MC4	1.78	1.145	2.43	0.425	2.1	0.0	0.0	0.9	1.2	19.3	3.7×10^{10}
			2.43	0.425	32.3	0.0	0.0	13.1	19.2		
MC5	1.81	1.119	2.44	0.446	1.6	0.0	0.0	0.6	0.9	19.1	3.6×10^{10}
			2.44	0.446	32.2	0.0	0.0	13.1	19.1		
MC6	1.81	1.122	2.44	0.433	2.1	0.0	0.0	0.9	1.2	19.1	3.7×10^{10}
			2.44	0.441	32.2	0.0	0.0	13.1	19.1		

S17 Spectroscopic informations about the BODIPYs used in the design Section

We note that to allow a direct comparison with the EET process using a zinc porphyrin, i.e., to compare with dyad **5**, we designed dyad **18** although its maximal absorption wavelength (688 nm) is not within the 700-770 region (red region).

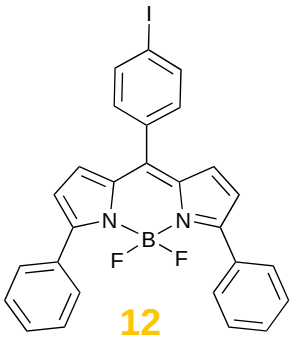

λ_{abs} = 558 nm; λ_{emi} = 592 nm
$CHCl_3$; Φ = 0.20

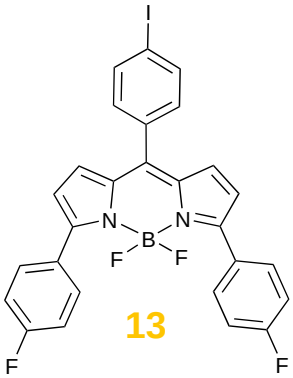

λ_{abs} = 555 nm; λ_{emi} = 590 nm
$CHCl_3$; Φ = 0.22

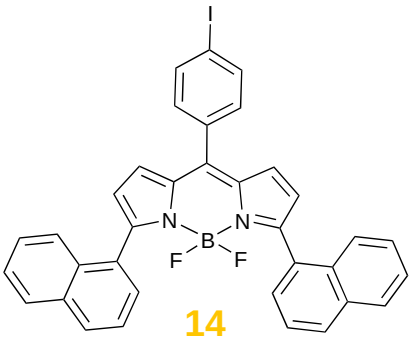

λ_{abs} = 542 nm; λ_{emi} = 607 nm
$CHCl_3$; Φ = 0.38

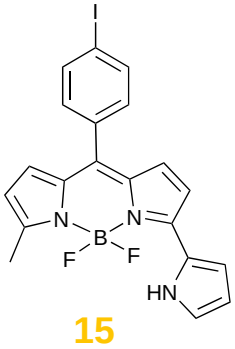

λ_{abs} = 573 nm; λ_{emi} = 600 nm
EtOH; Φ = 0.60

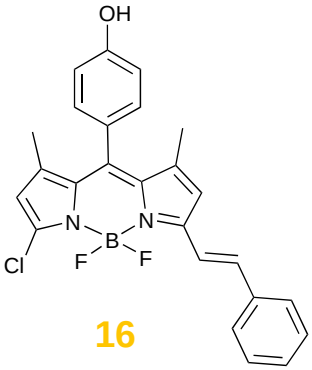

λ_{abs} = 564 nm; λ_{emi} = 579 nm
MeOH; Φ = 0.55

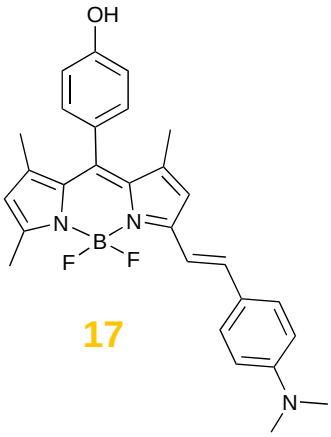

λ_{abs} = 565 nm; λ_{emi} = 660 nm
THF; Φ = 0.25

Fig. S14 Structure and spectroscopic information for the BODIPYs used in the designed dyads **12**-**17**. These data have been extracted from Refs. 1 (for **12** and **15**) and 2 (for **13**–**14** and **16**–**17**).

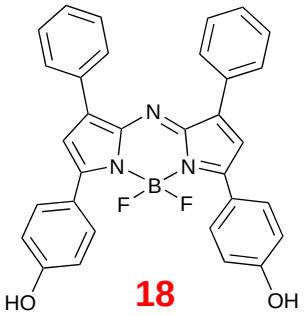

18

λ_{abs} **= 688nm**; λ_{emi} = 715 nm
$CHCl_3$; Φ = 0.36

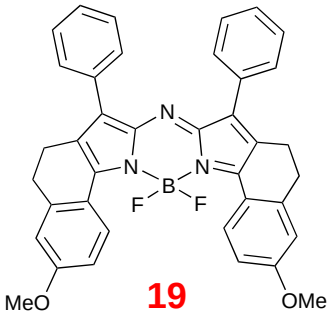

19

λ_{abs} **= 740 nm**; λ_{emi} = 751 nm
$CHCl_3$; Φ = 0.28

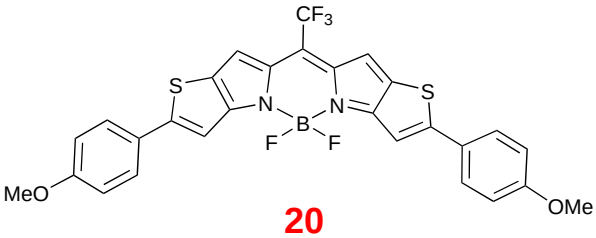

20

λ_{abs} **= 731 nm**; λ_{emi} = 754 nm
$CHCl_3$; Φ = 0.37

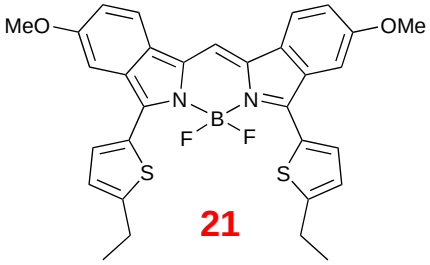

21

λ_{abs} **= 727 nm**; λ_{emi} = 780 nm
CH_2Cl_2; Φ = 0.20

Fig. S15 Structure and spectroscopic information for the BODIPYs used in the designed dyads **18**-**21**. These data have been extracted from Refs. 2 (for **18**) and 1 (for **19**–**21**).

S18 Fragment definition in ACP-BODIPY dyads

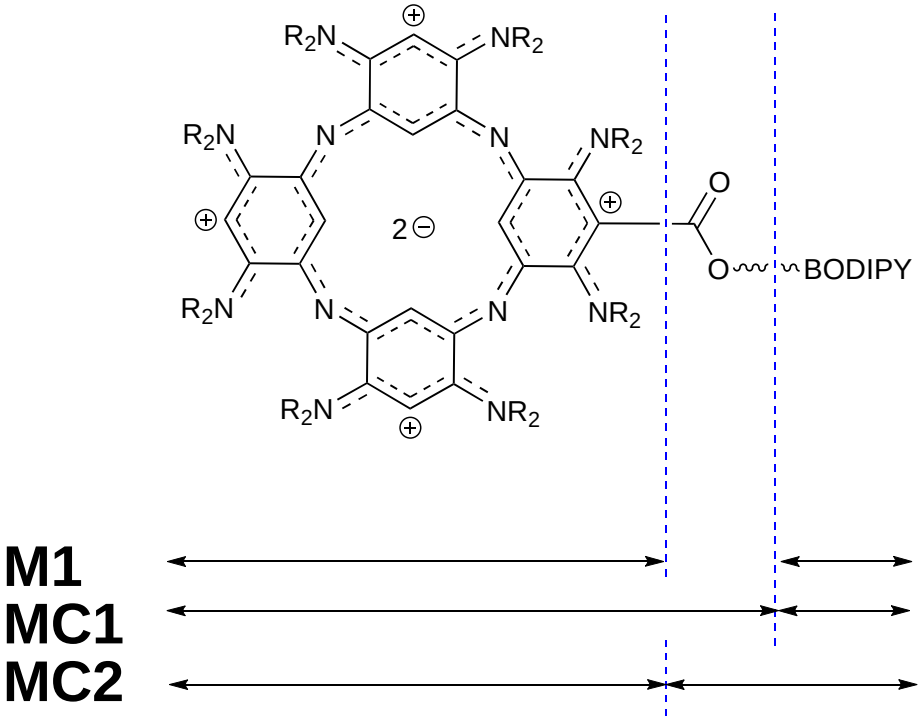

Fig. S16 Representation of the different fragmentation schemes considered in dyad **12** (R=H) and **12-Me** (R=CH_3).

S19 Comparisons between 12 and 12-Me: structures and EET couplings

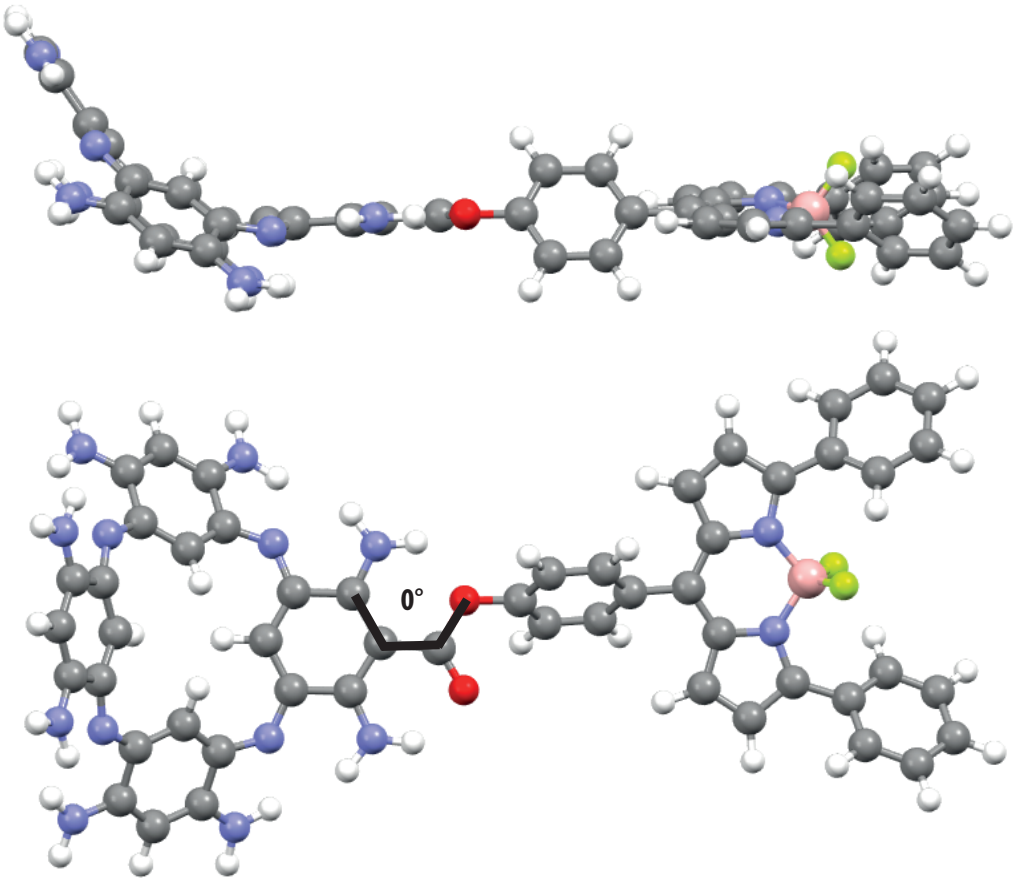

Fig. S17 Side (top) and top (bottom) views of the optimised structure of dyad **12**.

Table S17 Calculated transition energies ($\Delta E^{th.}_{abs}$ in eV) and oscillator strengths (f) of the excited-states of the different fragments involved in the electronic coupling in **12**. Theoretical absolute couplings (V in cm^{-1}) and EET rate constant ($k^{th.}$ in s^{-1}) computed on the fully-optimised structure for each fragmentation scheme (see Figure S16) are also given.

Fragmentation scheme	BODIPY fragment		ACP fragment		EET Coupling						
	$\Delta E^{th.}_{abs}$	f	$\Delta E^{th.}_{abs}$	f	V^{coul}	V^{xc}	V^{ovlp}	V^{PCM}	V^{tot}	V^{Whole}	$k^{th.}$
M1	2.50	0.702	2.07	0.395	57.3	0.0	0.0	24.3	33.0	33.0	3.0×10^{11}
			2.07	0.392	3.2	0.0	0.0	2.0	1.2		
MC1	2.49	0.702	2.06	0.399	18.3	0.2	0.0	8.2	10.2	38.6	4.2×10^{11}
			2.09	0.438	63.7	0.0	0.0	26.5	37.2		
MC2	2.48	0.697	2.07	0.395	57.2	0.0	0.0	24.0	33.2	33.2	3.1×10^{11}
			2.07	0.392	3.1	0.0	0.0	1.7	1.4		

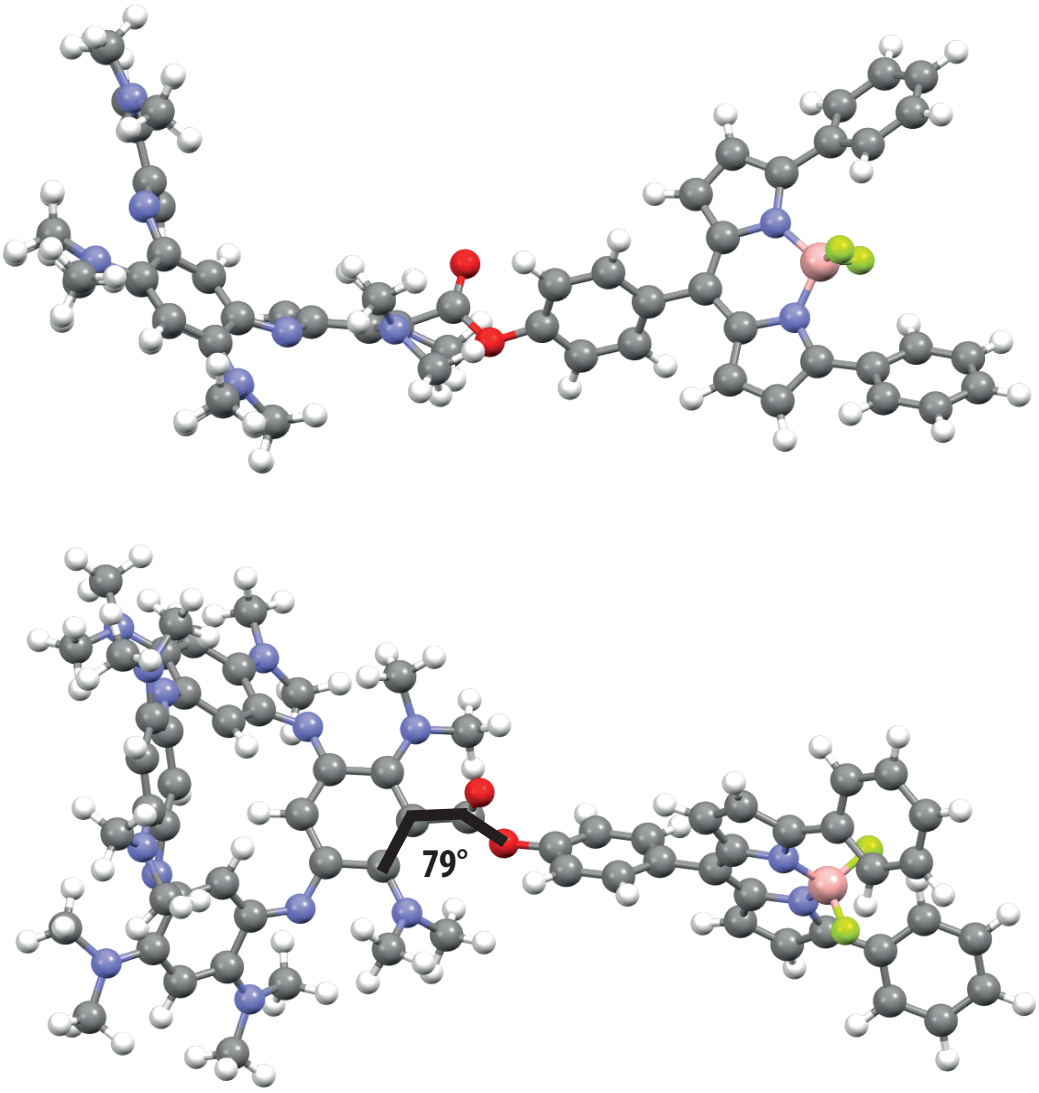

Fig. S18 Side (top) and top (bottom) views of the optimised structure of dyad **12-Me**.

Table S18 Calculated transition energies ($\Delta E_{abs}^{th.}$ in eV) and oscillator strengths (f) of the excited-states of the different fragments involved in the electronic coupling in **12-Me** (see Figure S16). Theoretical absolute couplings (V in cm^{-1}) and EET rate constant ($k^{th.}$ in s^{-1}) computed on the fully-optimised structure for each fragmentation scheme (see Figure S16) are also given.

Fragmentation scheme	BODIPY fragment		ACP fragment		EET Coupling						
	$\Delta E_{abs}^{th.}$	f	$\Delta E_{abs}^{th.}$	f	V^{coul}	V^{xc}	V^{ovlp}	V^{PCM}	V^{tot}	V^{Whole}	$k^{th.}$
M1	2.50	0.700	1.80	0.301	9.6	0.0	0.0	4.8	4.8	13.9	5.5×10^{10}
			1.86	0.308	22.6	0.0	0.0	9.6	13.0		
MC1	2.50	0.700	1.81	0.339	12.9	0.0	0.0	5.9	6.9	12.2	4.2×10^{10}
			1.86	0.294	18.1	0.1	0.0	7.9	10.1		
MC2	2.48	0.694	1.80	0.301	9.8	0.0	0.0	4.7	5.1	13.6	5.2×10^{10}
			1.86	0.308	22.5	0.0	0.0	9.9	12.6		

S20 Rotational analysis in dyad 12

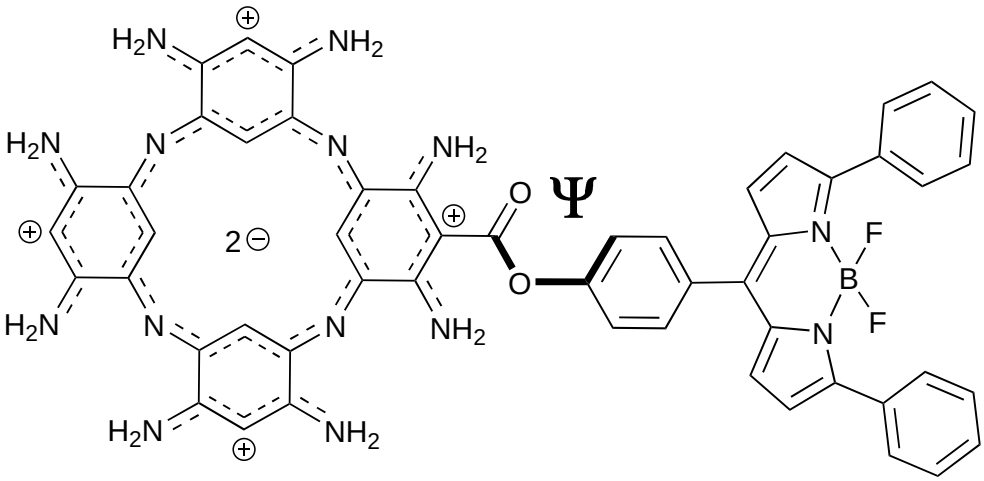

Fig. S19 Representation of the dihedral angle Ψ considered in the rotational analysis.

Table S19 Theoretical absolute total couplings (V^{Whole} in cm^{-1}) in dyad **12** when incrementing by 30° the Ψ dihedral angle between the two *meso* phenyls linked through the ethynyl bridge. The value of the angle Φ between the planes of the BODIPY and ZnP as well as the relative electronic energies ($E_{\mathrm{rel.}}$ in kcal/mol). The angles are given in degrees. Note that the 0° value corresponds to the fully-optimised geometry. The **MC2** fragmentation is applied.

Increment on Ψ	Angle Ψ	Angle Φ	$E_{\mathrm{rel.}}$	V^{Whole}
0	-120	26	0.0	33.2
30	-90	45	0.0	19.0
60	-60	70	0.1	11.7
90	-30	85	1.1	6.7
120	0	62	2.3	26.5
150	30	33	1.0	32.2

S21 Additional EET data for 12–21

Table S20 Theoretical absolute couplings (V in cm^{-1}) used to compute the total coupling and EET rate constant in the fully-optimised dyads **12–21** reported in Table 7 using the **MC2** fragment definition (see Figure S16). The magnitude of the transition dipole moment of the first transition of the BODIPY fragment ($\mu^{\mathrm{tr}}_{\mathrm{BODIPY}}$ in atomic units) is also given.

Dyad	BODIPY/ACP states	V^{coul}	V^{xc}	V^{ovlp}	V^{PCM}	V^{tot}	$\mu^{\mathrm{tr}}_{\mathrm{BODIPY}}$
12	S_1/S_3	57.2	0.0	0.0	24.0	33.2	3.4
	S_1/S_4	3.1	0.0	0.0	1.7	1.4	
13	S_1/S_3	56.8	0.0	0.0	23.8	33.0	3.4
	S_1/S_4	4.9	0.0	0.0	2.4	2.5	
14	S_1/S_3	48.9	0.0	0.0	20.7	28.2	3.2
	S_1/S_4	11.9	0.0	0.0	5.4	6.4	
15	S_1/S_3	88.6	0.2	0.0	38.2	50.2	3.6
	S_1/S_4	103.6	0.5	0.0	48.6	54.5	
16	S_1/S_3	43.7	0.0	0.0	18.4	25.3	4.0
	S_1/S_4	60.5	0.3	0.0	27.8	32.4	
17	S_1/S_3	25.8	0.1	0.0	10.7	15.1	5.0
	S_1/S_4	186.7	0.8	0.0	88.1	97.9	
18	S_1/S_1	100.5	0.8	0.0	41.4	58.3	4.3
	S_1/S_2	46.8	0.0	0.0	19.9	26.9	
19	S_1/S_1	125.7	1.0	0.0	51.4	73.4	4.5
	S_1/S_2	50.2	0.1	0.0	21.2	28.9	
20	S_1/S_1	148.8	0.8	0.0	64.9	83.1	6.0
	S_1/S_2	28.9	0.1	0.0	12.6	16.2	
21	S_1/S_1	135.6	0.6	0.0	57.4	77.7	4.2
	S_1/S_2	40.0	0.1	0.0	16.7	23.2	

S22 EET coupling in dyad 12-asym and 15-sym

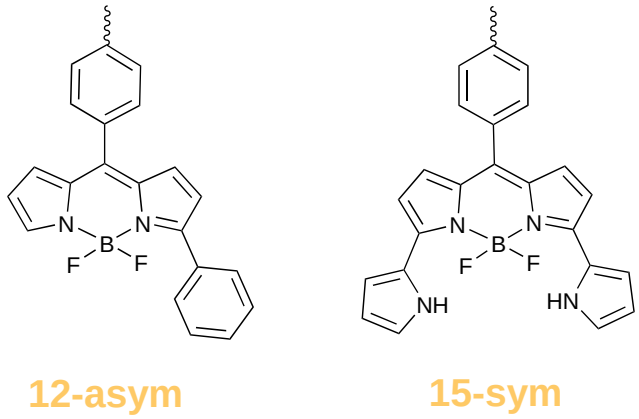

Fig. S20 Representation of the BODIPY units **12-asym** and **15-sym**.

Table S21 Calculated transition energies ($\Delta E^{th.}_{abs}$ in eV) and oscillator strengths (f) of the excited-states involved in the electronic coupling in **12-asym** and **15-sym** (see Figure S20). Theoretical absolute couplings (V in cm^{-1}) and magnitude of the transition dipole of the first excitation of the BODIPY (μ^{tr}_{BODIPY} in atomic units) are also given. The **MC2** fragmentation scheme (see Figure S16) has been used.

Dyad	BODIPY fragment			ACP fragment		EET Coupling					
	$\Delta E^{th.}_{abs}$	f	μ^{tr}_{BODIPY}	$\Delta E^{th.}_{abs}$	f	V^{coul}	V^{xc}	V^{ovlp}	V^{PCM}	V^{tot}	V^{Whole}
12-asym*	2.69	0.716	3.3	2.07	0.395	37.4	0.0	0.0	15.2	22.3	61.7
				2.07	0.392	104.6	0.6	0.0	46.4	57.6	
12-asym$^{\diamond}$	2.68	0.706	3.3	2.07	0.395	73.4	0.1	0.0	31.2	42.1	74.0
				2.07	0.392	111.9	0.7	0.0	50.3	60.9	
15-sym$^{\diamond}$	2.12	0.715	3.7	2.07	0.396	59.0	0.0	0.0	24.4	34.5	34.7
				2.07	0.393	7.1	0.0	0.0	3.0	4.0	

* not re-optimised
$^{\diamond}$ re-optimised

S23 Effect of the solvent change on the EET in dyad 5

Table S22 Calculated transition energies ($\Delta E^{th.}_{abs}$ in eV) and oscillator strengths (f) of the excited-states of the two fragments involved in the electronic coupling in **5** using the **MC1** fragment definition (see Figure S8). Theoretical absolute couplings (V in cm^{-1}) and EET rate constant ($k^{th.}$ in s^{-1}) computed on the fully-optimised structure for two different solvent are also given.

Solvent	BODIPY fragment		ZnP fragment		EET Coupling						
	$\Delta E^{th.}_{abs}$	f	$\Delta E^{th.}_{abs}$	f	V^{coul}	V^{xc}	V^{ovlp}	V^{PCM}	V^{tot}	V^{Whole}	$k^{th.}$
toluene$^{\diamond}$	1.99	0.865	2.31	0.047	74.8	1.1	0.0	34.7	39.0	39.0	4.3×10^{11}
			2.32	0.027	5.3	0.0	0.0	3.1	2.2		
dimethylsulfoxide$^{\diamond}$	2.00	0.845	2.31	0.053	77.0	1.2	0.0	32.3	43.5	43.7	5.4×10^{11}
			2.31	0.031	6.8	0.0	0.0	3.5	3.4		
dimethylsulfoxide*	2.00	0.844	2.30	0.066	81.1	1.2	0.0	33.5	46.5	46.5	6.1×10^{11}
			2.31	0.030	1.4	0.0	0.0	0.7	0.7		

$\diamond$ computed on the geometry optimised in toluene.
$\star$ computed on the geometry optimised in dimethylsulfoxide.

References

1 Y. Ni and J. Wu, *Org. Biomol. Chem.*, 2014, **12**, 3774–3791.
2 A. Loudet and K. Burgess, *Chem. Rev.*, 2007, **107**, 4891–4932.